Journal of Thermal Analysis and Calorimetry
https://doi.org/10.1007/s10973-020-09966-4

# Energy, exergy, economic analysis and optimization of single-effect absorption chiller network

**F. Panahizadeh[1] · M. Hamzehei[1] · M. Farzaneh-Gord[2] · A. A. V. Ochoa[3]**

Received: 4 May 2020 / Accepted: 15 June 2020


**Abstract**
This study is aimed to conduct energy, exergy and economic analysis on a network of single-effect absorption chillers. First, the network was analyzed parametrically and then optimized to minimize exergy destruction and annual cost. Multi-objective optimization was performed by implementing a particle swarm optimization algorithm. The case study was conducted on the absorption chiller network in Iranian Marun Petrochemical Company. The results indicated the greatest effects of the solution heat exchanger efficiency and network inlet cooling water temperature on energy and exergy performance coefficients and annual cost. Accordingly, decreasing the network inlet cooling water temperature from 35 to 25 °C increased energy and exergy performance coefficients by 5.3 and 6.2%, respectively, and reduced annual cost by $70,000.00. Besides, increasing solution heat exchanger efficiency from 60 to 80% increased energy and exergy performance coefficients by 5.9 and 2.1%, respectively, and decreased the annual cost by $60,000.00. According to the optimization results, the economic function of the network saved 9.95%, so that if the network works in optimized thermodynamics and economic conditions, the cost decreases by 3.24% compared to the typical manner.

**Keywords** Exergy and economic analysis · Absorption chiller network · Multi-objective optimization · Particle swarm optimization · Annual cost

**Abbreviations**

| | |
|---|---|
| $A$ | Area ($m^2$) |
| AOC | Annual operating and maintenance cost ($) |
| $C$ | Cost ($) |
| $C_P$ | Specific heat (kJ $kg^{-1}$ $K^{-1}$) |
| COP | Energy coefficient of performance |
| $D$ | Diameter (m) |
| $\dot{E}$ | Exergy flow rate (kW) |
| ECOP | Exergy coefficient of performance |
| ex | Exergy (kJ/kg) |
| $h$ | Enthalpy (kJ $kg^{-1}$) |
| $h$ | Heat transfer coefficient (kW $m^{-2}$ $K^{-1}$) |
| HX | Heat exchanger |
| $K$ | Thermal conductivity (kW $m^{-2}$ $K^{-1}$) |
| $L$ | Length (m) |
| LHV | Lower heat value (kJ $kg^{-1}$) |
| $\dot{m}$ | Mass flow rate (kg $s^{-1}$) |
| $\dot{M}$ | Mass flow rate (kg $s^{-1}$) |
| N | Equipment lifetime (year) |
| Nu | Nusselt number |
| $\Delta P$ | Pressure difference (kPa) |
| P | Pressure (kPa) |
| PF | Power factor (kW $TR^{-1}$) |
| Pr | Prantl number |
| $\dot{Q}$ | Heat transfer rate (kW) |
| Re | Reynolds number |
| $R_P$ | Control signal of pump under the current condition |
| s | Entropy (kJ $kg^{-1}K^{-1}$) |
| T | Temperature (°C) |
| $t$ | Time (s) |
| TR | Ton of refrigeration |
| $U$ | Overall heat transfer coefficient (kW $m^{-2}$ $K^{-1}$) |
| $\dot{W}$ | Electrical power (kW) |
| $X$ | Mass fraction |
| $\underline{Z}$ | Cost ($) |
| $z_e$ | Price of electrical power ($ $kW^{-1}$ $h^{-1}$) |
| $z_f$ | Price of fuel ($ $GJ^{-1}$) |

✉ M. Hamzehei
mahdi.hamzei@gmail.com; mahdi_hamzei@iauahvaz.ac.ir

[1] Department of Mechanical Engineering, Ahvaz Branch, Islamic Azad University, Ahvaz, Iran

[2] Department of Mechanical Engineering, Ferdowsi University of Mashhad, Mashhad, Iran

[3] Federal Institute of Technology of Pernambuco, Av. Prof. Luiz Freire 500, CEP:50740-540 Recife, PE, Brazil

Published online: 08 July 2020

**Greek symbols**

| | |
|---|---|
| $\beta$ | Maintenance factor |
| $\Gamma$ | Mass flow rate (kg $m^{-1}s^{-1}$) |
| δ | Solution film thickness (m) |
| η | Efficiency (%) |
| μ | Dynamic viscosity (N s $m^{-2}$) |
| φ | Relative humidity (%) |
| ω | Absolute humidity (%) |

**Subscripts**

| | |
|---|---|
| 1,2,3, … | Location in the water/steam side of cycle |
| a | Air |
| ACNP | Absorption chiller network plant |
| AC | Absorption chiller |
| ACN | Absorption chiller network |
| ABS | Absorber |
| b | Boiler |
| bf | Boiler fan |
| c | Combustion |
| C | Cooling |
| CD | Cooling demand |
| Ch | Chemical |
| chwni | Chilled water inlet network |
| chwno | Chilled water outlet network |
| chwp | Chilled water pump |
| CT | Cooling tower |
| cwf | Cooling tower fan |
| cwp | Cooling tower pump |
| cwni | Cooling water inlet network |
| D | Destruction |
| e | Electrical |
| EVA | Evaporator |
| EV | Expansion valve |
| envs | Environmental |
| f | Fuel |
| I | Inlet |
| I | Inner |
| hxo | Heat exchanger outlet |
| o | Outlet |
| o | Outer |
| O&M | Operation and Maintenance |
| P | Pump |
| ph | Physical |
| rated | The rated parameter |
| S | Steam |
| SHX | Solution heat exchanger |
| sol | Solution ($LiBr/H_2O$) |
| stni | Steam inlet network |
| t | Total |
| wb | Wet bulb |
| *w* | Water |
| 0 | Dead state |

## Introduction

The global economy has grown rapidly over the past few decades, largely due to the performance of industries. Generally, industries require a large amount of input energy, which causes problems in energy consumption and $CO_2$ emission. A large amount of energy is transmitted into the environment in different forms, such as waste heat. Compared to other refrigeration equipment, absorption chillers and/or heat pump have been widely used in industries, due to their ability to use waste heat or renewable energy to generate hot and chilled water [1–4]. These types of chillers due to using the cogeneration concept for their activation are more durable and energy efficient in comparison with the existing ones [5].

So far, many kinds of research have been carried out to evaluate the performance of absorption chillers or heat pumps based on energy and exergy analysis [6–9]. Ochoa et al. [10] in their work studied the first and second laws of thermodynamics to estimate the performance of an energy micro-cogeneration plant by coupling an absorption refrigeration system to supply chilled water for air-conditioning purposes. In the same context, comparing five different types of absorption chillers by using the first and second laws of thermodynamics, Maryami and Dehghan [11] found that the energetic and exergetic COPs increase for all absorption chillers types while the total exergy change decreases approximately. Applying the same thermodynamic principles, Petela and Szlek [12] carried out an energetic and exergetic analysis in the water/ammonia absorption chiller powered by solar energy to verify the thermal potential of producing cold, presenting a COP of 0.444 and an exergetic efficiency of 0.026. To further study the application of the second law of thermodynamics, several authors have been applied an advanced concept of this law to explore different energy systems, as seen in the literature [13, 14].

The methodology of thermodynamic analysis on the energy system has been applied in the industrial, residential and commercial sectors to verify its performance and technical viability [15, 16]. Hence, in Silva et al. [17] a cogeneration plant to meet the electrical and thermal demands in the rectory building section of a university campus was proposed. The used system included an internal combustion engine, a thermal boiler, a gas microturbine, a storage buffer vessel and an absorption refrigeration system to eliminate extra heat. That system had benefits to supply the required electricity and air-conditioning demand of university with improved overall efficiency. Applying the same methodology to verify the flexibility and operability of absorption chillers in tropical climates, Lubis et al. [18] analyzed the influence of maximizing the single- and double-effect absorption chiller COP through thermodynamic and experimental

studies. This work showed excellent improvement in system performance of 12 to 60% compared to a double-effect configuration. Lu et al. [19] proposed a prototype of an absorption heat pump using water/ammonia with an intermediate heat process, which uses low-quality heat of the environment and combustion chamber's outlet heat of the main and intermediate evaporators, respectively. Searching at south America countries, specifically in Brazil, Alcantara et al. [20] performed a financial investigation of an energy polygeneration plant considering an ice cream manufactory as a case study. The best scenario analyzed for the ice cream factory was presented with a good financial return with NPV of US$269,390.40, IRR of 26.32% and a payback of 3.4 years.

Another important studied aspect of the absorption refrigeration system is to use solar energy, renewable energy, for the activation of systems [21–23]. In this context, Sokhansefat et al. [24] carried out a transient analysis of a solar absorption cooling system installed and operated in the city of Tehran in Iran using the TRNSYS computational platform. Results showed that there is a possibility to improve the energy performance of the system by 28%, considering optimal values of the collector area (55 $m^2$), storage tank volume (1 $m^3$), boiler temperature adjustment (77 °C), the mass flow of the solar collector of 1000 kg $h^{-1}$ and a collector inclination of 33°. Taking advantage of the temperature drop in the cooling production, Arabkoohsar and Andresen [25] proposed to integrate a natural gas expansion station with an absorption chiller at the gas station. Results showed that the station could provide 27% cold per year and therefore use the hybrid system instead of the conventional chiller.

Due to the high energy demand for activating absorption chillers in district cooling, it is necessary to use highly efficient solar energy systems; therefore, Arabkoohsar and Sadi [26] proposed to use trough parabolic solar collectors to meet the demand for a cooling and district heating network. Using artificial neural network (ANN) and adaptive neuro-fuzzy inference system (ANFIS), Esen et al. [27] presented a comparative thermodynamic study of a solar heat pump system where the goal was to verify the performance of the type ground heat exchanger as a ground source to drive and it was found that the ANFIS was more appropriate than that of ANN for predicting the performance of system.

An important aspect in energy systems is the operation in conditions where efficiency is maximum and energetic consumption is as low as possible in order to make the most of energy inputs, such as fuels and solar energy [28]. Therefore, optimization is an essential tool in the correct operation and control in energy plants, such as off-grid hybrid solar and diesel systems to determinate the correct capacity and technology to work in the different areas [29, 30] to give an alternative choice to produce electricity in any remote location by combining renewable and/or non-renewable sources energies to do it. In another case, it is seen in generation plants that use fossil fuel as source input [31] or even by proposing a novel power generation plant to take advantage of the energies of geothermal hot water and liquid natural gas streams to produce power by using a combination of Kalina and Organic Rankine Cycles to achieve the best performance of producing power, as it has seen in Sadaghiani et al. [32], where first and second laws of thermodynamic analysis were conducted to made it. This also can see it in the work presented by Pakatchian et al. [33] where an optimization study to enhance the performance and operating stability of an axial compressor by using artificial neural network and computational fluid dynamics was carried out. Regarding absorption chiller systems, the optimization technique had been used to find the best configuration aiming for energetic and economic criteria, as seen in Pandya et al. [34] where thermodynamic modeling of single-stage absorption cooling system integrated with different solar collector types was made. In the same context of absorption refrigeration systems, Pandya et al. [35] presented an energetic study to compare the performance of solar absorption chillers that uses ammonia and two different absorbents: sodium thiocyanate and lithium nitrate, to verify the best collector solar systems under energetic and financial criteria where it was found that the $NH_3/LiNO_3$ coupled with evacuated tube collector was superior to any others technologies analyzed.

The lack of efficient operation in real time as the main problem of the absorption chillers network highlights the need for a good control strategy [36]. Hence, researchers have been looking for optimal control strategies that can provide maximum efficiency without increasing the cost of operation and repairment of equipment [37]. In the context of maximizing the energy efficiency of chilled water-cooling systems in real time, Mu et al. [38] proposed an optimization strategy considering a multivariate control of the search for extremes with penalty terms. The proposed strategy was evaluated using a dynamic model built and simulated in Modelica considering an ice water plant with two parallel chillers. Huang et al. [39] considered a compression chiller plant to present a model to verify the effect of cooling tower water temperature set point on the cooling load control by using the Hooke Jeeves optimization algorithm.

The energy costs for the activation and maintenance of ventilation and air-conditioning systems are very high. Therefore, there is a need to improve energy efficiency, through the implementation of an optimized control and supervision system, as seen in Wang et al. [40] where it was recommended and tested a predictive optimization method based on the prediction of the cooling load to address this problem. In this regard, most methods used to optimize the chillers network plant include optimizing the heat load division between the chillers of the network and the number of ON chillers in the network [41]. Other researchers have

used innovative methods based on genetic search algorithms [42] or swarm intelligent algorithm [43] and also incorporate optimal values of operational variable settings to perform a time-dependent control, such as the Bayesian networks [44] and using and artificial neural network methods [45].

Despite extensive research on absorption chiller and compression chiller networks, a few kinds of research have been conducted on the single-effect steam absorption chiller network plant combining the thermodynamics, economic and optimization analysis. Thus, the present study aims to carry out energy, exergy and economic optimization analysis on the network of single-effect absorption chillers. The system was analyzed parametrically and optimized to maximize exergy performance coefficient and minimize annual cost. The governing equations were solved using advanced programming in engineering equations solver, while multi-objective optimization was performed by implementing particle swarm optimization algorithm in MATLAB software. A case study was carried out on the absorption chiller network plant in Marun Petrochemical Company in Iran. In addition to the 3E analysis which, according to the open literature, has not previously been performed for the single-effect steam absorption chiller network plant which compromised electrical and thermal energy consumption, another innovation of the present study is the use of particle swarm optimization algorithm to select the optimal operating conditions of the plant. The results obtained from the present study for the absorption chiller network plant with high cooling capacity with industrial application clearly show that the mentioned method can be used with good accuracy for this plant and cause a significant reduction in the plant annual cost. The results of this study can help to improve the utilization of the absorption chiller network plant with more reliability and increase its efficiency.

## Analysis and modeling of absorption chiller network plant

This section describes the plant to be analyzed considering the main components. The energetic and exergetic modeling of the system is presented including the economic aspects involved in the modeling and study of the plant.

### Absorption chiller network plant

As shown in Fig. 1a, the absorption chiller network plant (ACNP) has an absorption chiller network (ACN) containing more than one absorption chillers working in series or in parallel to provide the required cooling load. The plant should have additional equipment including the main boiler, chilled water storage tank, cooling tower, cooling water pump, chilled water pump and air handling or heat exchangers to generate cooling demand required in the process.

Concerning the ACNP function, heat is given to the chilled water in heat exchangers or air conditioners. The chilled water heated in the air conditioners is stored in a storage tank, sucked by the chilled water pump and conveyed to the ACN to be divided into several chillers. On the other hand, the heat generated by the boilers is sent to the generator of chillers to heat the LiBr/$H_2O$ solution as shown in Fig. 1b, resulting in obtaining a denser solution.

After passing the heat through the drain exchanger and preheating the outlet dilute solution from the primary exchanger, the steam that has lost some of its heat is condensed and sent to the boiler. Further, cooling water absorbs part of the heat of LiBr/$H_2O$ solution in the absorber of chillers and, thus, increases its absorption power and condenses the refrigerant vapors in the condenser of chillers. The gravity of the condenser transfers the condensed refrigerant to the evaporator of the chillers for spraying on chilled

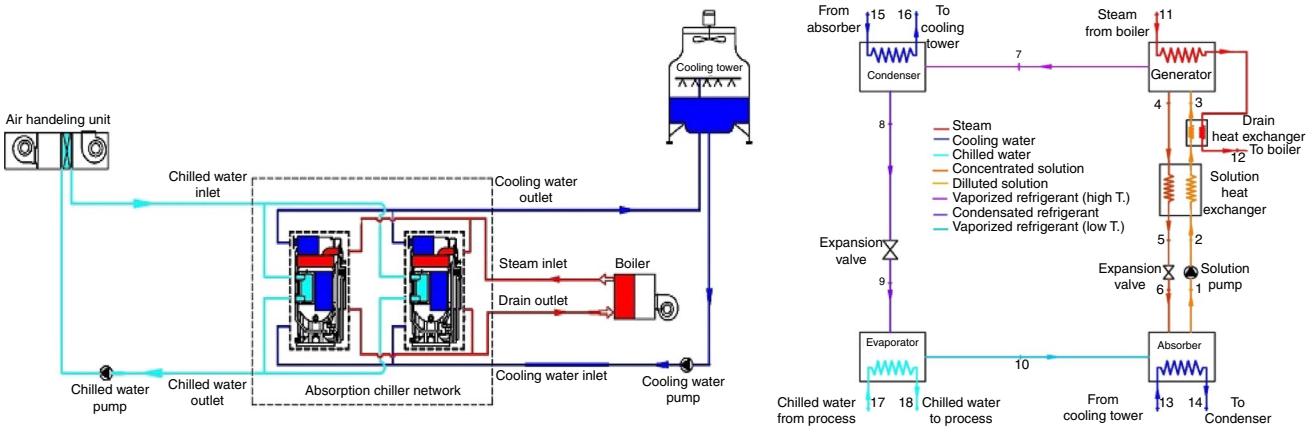


**Fig. 1** **a** The schematic of an ACNP. **b** The schematic of heat flow in a single-effect steam absorption chiller

water tubes and cools the chilled water. The cooling water is heated in the absorber, and the condenser of chillers is sent to the cooling tower for cooling. The steam generated in the process enters the ACN. By exchanging heat in the generator of chillers network with LiBr/$H_2O$ solution and accelerating the separation of refrigerant from the solution, the steam is condensed and sent back to the condensation tank.

## Analysis of the single-effect steam absorption chiller

To model the absorption chiller network (ACN), first, the chiller was modeled then generalized to the chillers network. To apply the mass and energy balance to each part of the single-effect absorption was developed to determine the performance of the system. The assumptions considered for modeling process are used along other works presented in the literature [2, 5], as follows:

- The steady-state analysis is carried out, and the working fluid is LiBr/$H_2O$ solution.
- Exchanges of heat with the neighborhood are negligible.
- The temperature, pressure and concentration in each component are homogeneous.
- There are only two pressure ranges that are high pressure (generator and condenser) and low pressure (absorber and evaporator).
- Refrigerant pump power is insignificant.
- The LiBr/$H_2O$ solution leaves the generator, and the pump is in a saturated state.
- The Expansion valve is considered adiabatic, and its process is isentropic.
- Kinetic and potential energy changes are negligible.
- Chiller heat exchanger efficiency is constant.
- The drain heat exchanger is considered a part of the generator, and it is assumed that the steam output is completely condensed.

### Energy analysis of the single-effect absorption chiller

The equations of mass and energy balance for each component of the single-effect absorption chiller considering assumptions made are shown in Table 1.

The energy coefficient of performance (COP) of absorption chiller is calculated using the following equation [46].

$$\mathrm{COP}_{\mathrm{AC}} = \frac{\dot{Q}_{\mathrm{EVA}}}{\dot{Q}_{\mathrm{GEN}} + \dot{W}_{\mathrm{P}}} \tag{1}$$

where $\dot{Q}_{\mathrm{EVA}}, \dot{Q}_{\mathrm{GEN}}$ and $\dot{\mathrm{W}}_{\mathrm{P}}$ are heat transfer in the evaporator, generator and chiller's pump power consumption, respectively.

**Table 1** The equations of mass and energy balance in the single-effect absorption chiller

| Equipment | Equation |
|---|---|
| Generator | $\dot{m}_{\mathrm{ws}}X_{\mathrm{ws}} + \dot{m}_{\mathrm{r}} = \dot{m}_{\mathrm{ss}}X_{\mathrm{ss}}$ |
| | $\dot{m}_3h_3 + \dot{Q}_{\mathrm{GEN}} = \dot{m}_4h_4 + \dot{m}_7h_7$ |
| Absorber | $\dot{m}_{\mathrm{ws}}X_{\mathrm{ws}} + \dot{m}_{\mathrm{r}} = \dot{m}_{\mathrm{ss}}X_{\mathrm{ss}}$ |
| | $\dot{m}_6h_6 + \dot{m}_{10}h_{10} = \dot{Q}_{\mathrm{ABS}} + \dot{m}_1h_1$ |
| Solution pump | $\dot{m}_1h_1 + \dot{W}_{\mathrm{P}} = \dot{m}_2h_2$ |
| Expansion valve 1 | $\dot{m}_5h_5 = \dot{m}_6h_6$ |
| Expansion valve 2 | $\dot{m}_8h_8 = \dot{m}_9h_9$. |
| Solution heat exchanger | $\dot{m}_2h_2 + \dot{m}_4h_4 = \dot{m}_3h_3 + \dot{m}_5h_5$ |
| Evaporator | $\dot{m}_{10}h_{10} + \dot{Q}_{\mathrm{EVA}} = \dot{m}_9h_9$ |
| Condenser | $\dot{m}_7h_7 = \dot{Q}_{\mathrm{CON}} + \dot{m}_8h_8$ |

**Table 2** The properties of the LiBr/$H_2O$ solution at zero point (dead State)

| Quantity | Value | Unit |
|---|---|---|
| $T_0$ | 298.15 | K |
| $P_0$ | 101.325 | kPa |
| $X_0$ | 0.48 | – |
| $h_0$ | 49.62 | kJ $kg^{-1}$ |
| $s_0$ | 0.1981 | kJ $kg^{-1}$ $K^{-1}$ |

### Exergy analysis of the single-effect absorption chiller

$$\dot{E}x_{\mathrm{Q}} + \sum_{\mathrm{i}} \dot{m}_{\mathrm{i}}ex_{\mathrm{i}} = \sum_{\mathrm{o}} \dot{m}_{\mathrm{o}}ex_{\mathrm{o}} + \dot{E}x_{\mathrm{W}} + \dot{E}x_{\mathrm{D}} \tag{2}$$

According to the second law of thermodynamics and the principles of exergy, the general relation of the exergy rate balance is written as follows [47, 48]:

$$\dot{E}x_{\mathrm{Q}} = \left(1 - \frac{T_0}{T_{\mathrm{i}}}\right)\dot{Q}_{\mathrm{i}} \tag{3}$$

$$\dot{E}x_{\mathrm{W}} = \dot{W} \tag{4}$$

where ex, $\dot{m}, \dot{E}x_{\mathrm{Q}}, \dot{E}x_{\mathrm{W}}$ and $\dot{E}x_{\mathrm{D}}$ are exergy, mass flow rate, exergy rate due to heat transfer at control volume boundary at absolute temperature, exergy rate related to shaft work and exergy destruction rate, respectively. The indexes i and o refer to inlet and outlet.

$$ex = ex_{\mathrm{ph}} + ex_{\mathrm{ch}} \tag{5}$$

$$ex_{\mathrm{ph}} = \left(h - h_0\right) - T_0\left(s - s_0\right) \tag{6}$$

Exergy is composed of physical ($ex_{\mathrm{ph}}$) and chemical ($ex_{\mathrm{ch}}$) exergies, and they are expressed as [47, 48]:where h and s are enthalpy and entropy, respectively. Index 0 refers to the dead state, and the dead state conditions of the present study are given in Table 2.

The chemical exergy of the LiBr/$H_2O$ solution was obtained from the following relation based on the mass fraction of the LiBr/$H_2O$ solution in (kJ $kg^{-1}$) [47, 48].

$$ex_{ch,LiBr/H_2O} = -500X^3 + 1291X^2 + 341.071X + 15.719 \quad (7)$$

The exergy destruction of the components of the absorption chiller is presented in Table 3.

The exergy destruction of the absorption chiller is expressed as:

$$\dot{E}_i = \dot{m}_i \times ex_i \quad (8)$$

$$\dot{E}_D^{AC} = \dot{E}_D^{GEN} + \dot{E}_D^{CON} + \dot{E}_D^{ABS} + \dot{E}_D^{EVA} + \dot{E}_D^{SHX} + \dot{E}_D^{EV1} + \dot{E}_D^{EV2} + \dot{E}_D^{SP} \quad (9)$$

Finally, the ECOP of absorption chiller is calculated using the following equation:

$$ECOP_{AC} = \frac{\dot{E}_{EVA}}{\dot{E}_{GEN} + \dot{E}_P} = 1 - \frac{\dot{E}_D^{AC}}{\dot{E}_{GEN} + \dot{E}_P} \quad (10)$$

where $\dot{E}_{EVA}$, $\dot{E}_{GEN}$, and $\dot{E}_P$ are exergy rate of heat transfer in evaporator, generator and exergy rate of power input to chiller's pumps, respectively.

## Thermodynamic modeling of the absorption chiller network plant

This section deals with the energy and exergy analysis of the absorption chiller network plant considering the assumptions made before.

### Energy analysis of the absorption chiller network plant

A heat source is required to produce the cold in the ACNP with single-effect chillers, which usually uses steam at temperatures below 150 °C and pressures less than 2 bars. The required heat source of the plant can be supplied in two ways. Firstly, natural gas or any other fuel in the steam boiler is used to generate steam, and in a second way, the waste heat could be used, which would result in a significant increase in plant efficiency due to reduced fuel consumption [49]. In addition to fuel, the ACNP also uses electricity for cooling tower water pumps, cooling tower fans, chilled water pumps and absorption chiller pumps. The total electrical power consumption of this plant is calculated as follows:

$$\dot{W}_{ACNP}(t) = \sum_{i=1}^{N} \left(\dot{W}_{AC}(i) + \dot{W}_{chwp}(i)\right) + \sum_{j=1}^{M} \left(\dot{W}_{cwf}(j) + \dot{W}_{cwp}(j)\right) + \sum_{k=1}^{L} \dot{W}_{bf}(j) \quad (kW) \quad (11)$$

In Eq. 11, $N$ is the number of absorption chillers, $M$ is the number of cooling towers, and $L$ is the number of steam boilers.

where $\dot{W}_{AC}$, $\dot{W}_{chwp}$, $\dot{W}_{cwp}$, $\dot{W}_{cwf}$ and $\dot{W}_{bf}$ are power consumption of absorption chiller, chilled water pump, cooling water pump, cooling tower fan and boiler fan, respectively.

$$\dot{W}_{cwf} = \frac{\dot{m}_{a,i} \times \Delta P_{cwf}}{\rho_{a,i} \times \eta_{cwf}} \quad (12)$$

In the above equation, $\dot{m}_{a,i}$, $\rho_{a,i}$, $\Delta P_{cwf}$ and $\eta_{cwf}$ are mass flow rate of inlet air, the density of inlet air, pressure difference across fan and efficiency of the fan.

$$\dot{W}_{bf} = \frac{\dot{m}_{a,i} \times \Delta P_{bf}}{\rho_{a,i} \times \eta_{bf}} \quad (13)$$

$$\dot{Q}_{ACNP} = \dot{Q}_b = \eta_c \times \dot{m}_f \times LHV_f \quad (14)$$

where $\dot{Q}_{ACNP}$, $\dot{m}_f$, $LHV_f$ and $\eta_c$ are thermal energy consumption of boiler, fuel mass flow rate, fuel lower heat value and combustion efficiency, respectively.

The following equation can be used to calculate the required cooling load [50]:

$$\dot{Q}_{cooling,t} = 0.2843 \times \dot{m}_{chw} \times C_{Pw} \times \left(T_{chwni} - T_{chwno}\right)(TR) \quad (15)$$

In the above relation, 0.2853 is the unit conversion factor for convert kilowatt to refrigeration ton and $\dot{m}_{chw}$, $C_{Pw}$, $T_{chwni}$ and $T_{chwno}$ are chilled water flow rate, the specific heat of water, chilled water inlet and outlet temperatures, respectively.

The $COP_{ACN}$ with N chillers is defined as follows:

$$COP_{ACN} = \frac{\dot{Q}_{Cooling,t}}{\sum_{j=1}^{N}(\dot{Q}_{GEN,j} + \dot{W}_{P,j})} \quad (16)$$

**Table 3** The exergy destruction of various components of the absorption chiller

| Component | Equation |
|---|---|
| Generator | $\dot{E}_D^{GEN} = \dot{E}_3 + \dot{E}_{11} - \dot{E}_4 - \dot{E}_7 - \dot{E}_{12}$ |
| Absorber | $\dot{E}_{ABS}^{GEN} = \dot{E}_{10} + \dot{E}_6 + \dot{E}_{13} - \dot{E}_1 - \dot{E}_{14}$ |
| Solution pump | $\dot{E}_D^{SP} = \dot{E}_2 - \dot{E}_1$ |
| Expansion valve 1 | $\dot{E}_5 - \dot{E}_6$ |
| Expansion valve 2 | $\dot{E}_D^{EV2} = \dot{E}_8 - \dot{E}_9$ |
| Solution heat exchanger | $\dot{E}_D^{SHX} = \dot{E}_4 + \dot{E}_2 - \dot{E}_5 - \dot{E}_3$. |
| Evaporator | $\dot{E}_D^{EVA} = \dot{E}_9 + \dot{E}_{17} - \dot{E}_{18} - \dot{E}_{10}$ |
| Condenser | $\dot{E}_D^{CON} = \dot{E}_7 + \dot{E}_{15} - \dot{E}_{16} - \dot{E}_8$ |

where $\dot{Q}_{Cooling,t}$, $\dot{Q}_{GEN}$ and $\dot{W}_P$ are a total cooling load of the network, ACN's generators heat input and ACN's pumps power input, respectively.

The $COP_{ACNP}$ is defined as follows:

$$COP_{ACNP} = \frac{\dot{Q}_{Cooling,t}}{\dot{Q}_{ACNP} + \dot{W}_{ACNP}} \tag{17}$$

### Exergy analysis of the absorption chiller network plant

The exergy destruction of the ACNP is equal to the total exergy destruction in the ACN, cooling towers and heat exchangers. The exergy destruction of the ACNP is obtained using the following equation.

$$\begin{aligned}\dot{E}_D^{ACNP} &= \dot{E}_D^B + \dot{E}_D^{ACN} + \dot{E}_D^{CT} + \dot{E}_D^{HX} + \dot{E}_D^{ST} \\ &= \sum_{i=1}^{M} \dot{E}_D^{B_i} + \sum_{j=1}^{N} \dot{E}_D^{AC_j} + \sum_{k=1}^{U} \dot{E}_D^{CT_k} + \sum_{l=1}^{V} \dot{E}_D^{HX_l} + \sum_{o=1}^{W} \dot{E}_D^{ST_o}\end{aligned} \tag{18}$$

In Eq. (18) the exergy destruction of ACNP's pumps and fans is assumed negligible.

where

$$\dot{E}_D^B = \dot{E}_{stno} - \dot{E}_{stni} + \dot{m}_{fuel} \times \dot{E}_{fuel} - \dot{E}_{fluegas} \tag{19}$$

$$\dot{E}_D^{CT} = \dot{E}_{cwno} - \dot{E}_{cwni} + \dot{E}_{air,i} - \dot{E}_{air,o} \tag{20}$$

$$\dot{E}_D^{HX} = \dot{E}_{chwni} - \dot{E}_{chwno} \tag{21}$$

$$\dot{E}_D^{ST} = \dot{E}_{chwhxo} - \dot{E}_{chwni} \tag{22}$$

In these relationships, $\dot{E}_D^{AC}$ is the exergy destruction of each absorption chiller and N represents the number of chillers in the network.

The $ECOP_{ACN}$ is defined as follows:

$$ECOP_{ACN} = 1 - \frac{\sum_j^N \dot{E}_D^{AC,\,j}}{\sum_j^N \left(\dot{E}_{GEN,\,j} + \dot{E}_{P,\,j}\right)} \tag{23}$$

The $ECOP_{ACNP}$ is equal to:

$$ECOP_{ACNP} = 1 - \frac{\dot{E}_D^{ACNP}}{\dot{m}_f \times ex_f + \dot{E}_{W_{ACNP}}} \tag{24}$$

where $\dot{m}_f$, $ex_f$ and $\dot{E}_{W_{ACNP}}$ are mass flow rate of fuel, the exergy of fuel and exergy rate associate with power input to ACNP.

### Economic analysis of the absorption chiller network plant

In the ACNP, the cost of fuel consumption is also important in addition to the cost of electricity consumed by the plant. In the present study, it was seeking to optimize the total annual operating and maintenance cost of the plant ($AOC_{ACNP}$). Therefore, $AOC_{ACNP}$ is calculated as follows:

$$AOC_{ACNP} = \beta \times C_{invs} + C_f + C_e \quad \left(\$year^{-1}\right) \tag{25}$$

where $\beta$, $C_{invs}$, $C_f$ and $C_e$ are maintenance factor, investment cost, fuel cost and electrical power cost, respectively.

In the above equation, the investment cost is calculated from the following relation [51]:

$$C_{invs} = \sum_{i}^{n} Z_i \tag{26}$$

The investment cost is spent on the purchase and installation of plant equipment, as shown in Table 4.

The price of equipment needs to be updated by using the newest chemical engineering plant cost index (CEPCI) and the following equation [52]:

$$Z_{2019} = Z_{\text{Reference year}} \times \left[\frac{\text{Cost ndex for 2019}}{\text{Cost index for reference year}}\right] \tag{27}$$

**Table 4** Cost function for ACNP's equipment [53, 54]

| Equipment name | Cost function (dollars) | Reference year |
|---|---|---|
| Condenser | $Z_{CON} = (516.62 \times A_{CON}) + 268.45$ | 1995 |
| Evaporator | $Z_{EVA} = (516.62 \times A_{EVA}) + 268.45$ | 1996 |
| Generator | $Z_{GEN} = (516.62 \times A_{GEN}) + 268.45$ | 1995 |
| Absorber | $Z_{ABS} = (516.62 \times A_{ABS}) + 268.45$ | 1995 |
| SHX | $Z_{SHX} = (516.62 \times A_{SHX}) + 268.45$ | 1995 |
| Pump | $Z_P = 705.48 \times \dot{W}_P^{0.71}\left(1 + \frac{0.2}{\eta_P}\right)$ | *2006* |
| Cooling tower | $Z_{CT} = 746.749 \times \dot{m}_{CT}^{0.71} \times \Delta T_{CT}^{0.57} (T_{i,CT} - T_{o,CT})^{-0.9924} \times (0.022 \times T_{wb,o} + 0.32)^{0.706}$ | 2017 |
| Steam boiler | $Z_B$ = Ton of Steam × 6500 | 2015 |

The cost of fuel and electrical power consumption is also calculated from the following relationships:

$$C_{\mathrm{f}} = \left(z_{\mathrm{f}} \times \dot{m}_{\mathrm{f}} \times \mathrm{LHV}\right) \times 3600 \times t_{\mathrm{year}} \tag{28}$$

$$C_{\mathrm{e}} = \left(z_{\mathrm{e}} \times \dot{W}_{\mathrm{elc}}\right) \times t_{\mathrm{year}} \tag{29}$$

where $z_{\mathrm{f}}, z_{\mathrm{e}}, \dot{W}_{\mathrm{elc}}$ and $t_{\mathrm{year}}$ are fuel price, electrical power price, electrical power consumption and the plant operating hour in a year, respectively.

### Implementation of the numerical modeling of the absorption chiller network

Numerical modeling of the ACN was performed with advanced high accuracy coding in EES [55]. According to the flowchart shown in Fig. 2, the equations of mass and energy balance are first written for the different components of each chiller network. By applying the inlet flow rates and temperatures (such as flow rates and temperatures of chilled water, cooling tower water and steam) and considering the UA of different chillers heat exchangers and the simultaneous solution of the equations given in Tables 1 and 3, the unknown values are calculated by the written numerical code.

## Optimization of the absorption chiller network plant

This section deals with the optimization processes applied in the absorption chiller network plant considering different parameters such as chilled and cooling water temperature. Optimization scenarios are presented, and the technique is employed in the modeling.

### Optimization scenarios

As shown in Fig. 3, different operating parameters are important in the performance of the ACNP from the viewpoint of exergy and energy analysis, as any change in these parameters changes the $\mathrm{COP}_{\mathrm{ACNP}}$ and $\mathrm{ECOP}_{\mathrm{ACNP}}$. In the compression chillers network, minimizing power factor (PF) is generally considered a criterion for the optimization process, because such networks only consume electricity [50]. Considering the consumption of fuel and electricity to

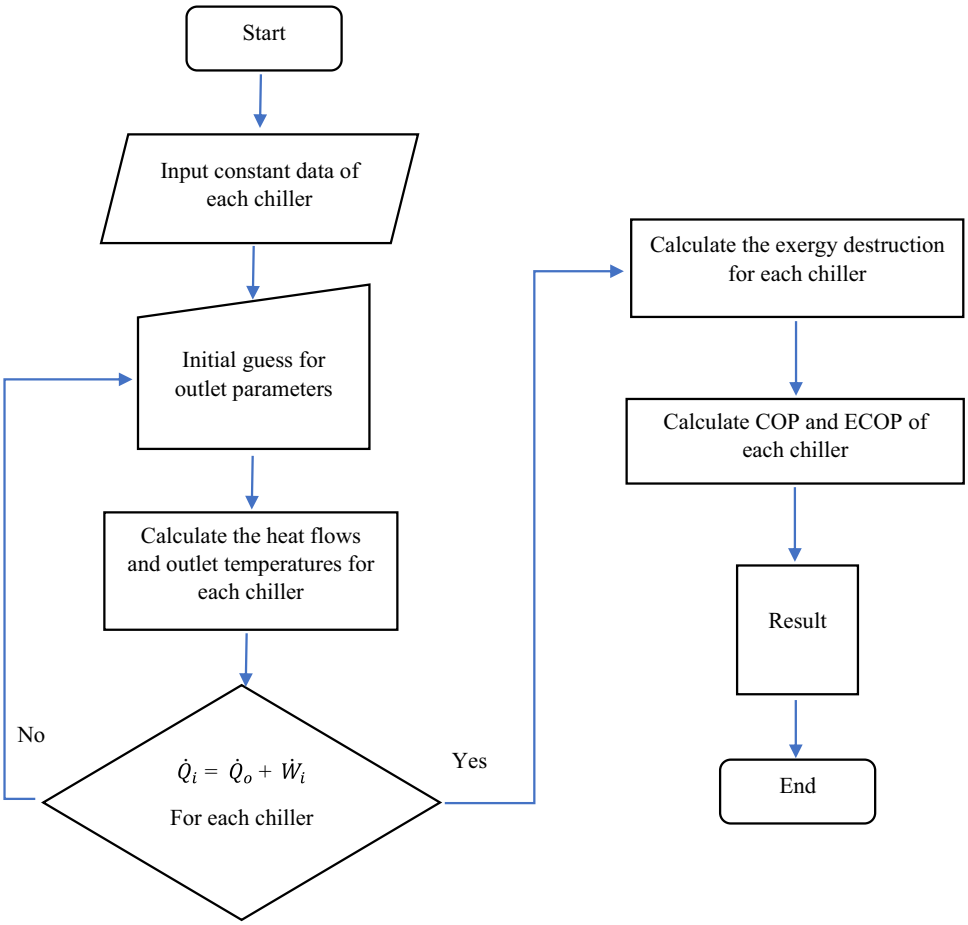


**Fig. 2** Flowchart for ACN modeling

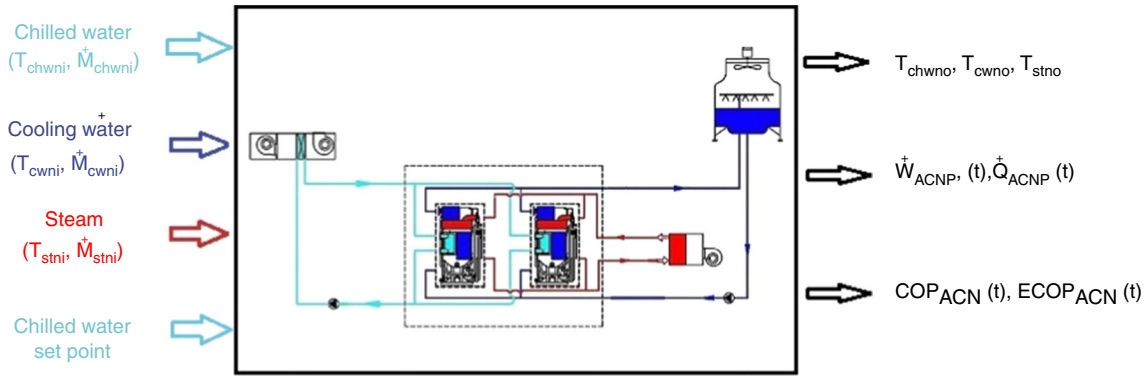


**Fig. 3** The schematic of ACNP model

produce steam in the ACN, the purpose is to maximize the exergy coefficient of performance and minimize the annual costs of the plant. To this aim, this study addresses various scenarios, which are presented subsequently.

Five scenarios of the simulation are presented to evaluate and optimize the system. The optimization scenarios are:

- The scenario of optimization the cooling water inlet temperature
- The scenario of ON and OFF network chillers
- The scenario of optimizing the chilled water temperature of the network outlet
- The Scenario of changing the inlet chilled water, cooling water and steam flow rate
- Combination of prior scenarios

### Scenario of optimization the cooling water inlet temperature

Decreasing the temperature of the cooling water leads to an increase in cooling capacity of the chiller network and a decrease in chilled water outlet temperature of the network. On the other hand, decreasing the temperature of the cooling water increases the $COP_{ACNP}$, and due to higher cooling tower fan operation, it increases plant electrical power consumption. It also declined fuel consumption in the boiler due to the reduced heat required in the chillers of network. Therefore, the cooling water temperature should be chosen in such a way that the rate of increase in plant cooling capacity is superior to the cost of electricity. The temperature of the cooling water should be adjusted to minimize the electrical power consumption of the ACNP's equipment and so that the minimum fuel consumption occurs in the boiler. Since the nature of these two types of energy is different, it was using the concept of exergy to represent it. Exergies of heat and work are calculated according to Eqs. (3) and (4) and are replaced by the following equation.

$$T_{\mathrm{cwni,set}}^{\mathrm{argmin}}\left(E_{\mathrm{t}}|_{t_0}^{t_0+\Delta t}\right)=\mathrm{minimum}\left(\int_{t_0}^{t_0+\Delta t}(\dot{E}_{\mathrm{W_{ACNP},t}}(t))\mathrm{d}t+\dot{E}_{\mathrm{Q_b}}(t)\mathrm{d}t\right)$$
$$t\in\left[t_0,t_0+\Delta t\right] \tag{30}$$

The electrical power consumption of the absorption chiller is not a function of the cooling water temperature, so it is ignored in the following equations.

$$\dot{E}_{\mathrm{Q_b}}(t)=F\left(T_{\mathrm{cwni}}(t),\dot{Q}_{\mathrm{c,t}}^{\mathrm{CD}}(t)\right) \tag{31}$$

$$\dot{E}_{\mathrm{W_{ct}}}(t)=F\left(T_{wb}(t),T_{\mathrm{cwni,set}}\left(t_0\right),T_{\mathrm{cwno}}(t)\right) \tag{32}$$

$$T_{\mathrm{cwni,set,L}}\le T_{\mathrm{cwni,set}}\left(t_0\right)\le T_{\mathrm{cwni,set,H}} \tag{33}$$

$$T_{\mathrm{cwni}}(t)=F\left(T_{\mathrm{wb}}(t),T_{\mathrm{cwni,set}}\left(t_0\right),T_{\mathrm{cwno}}(t)\right) \tag{34}$$

$$T_{\mathrm{cwno}}(t)=F\left(\dot{Q}_{\mathrm{c,t}}^{\mathrm{CD}}(t),\dot{Q}_{\mathrm{b}}(t),T_{\mathrm{cwni}}(t)\right) \tag{35}$$

In the above equations, $E_{\mathrm{t}}|_{t_0}^{t_0+\Delta t}$, $\dot{Q}_{\mathrm{c,t}}^{\mathrm{CD}}$ and $T_{\mathrm{wb}}$ are representatives of total input exergy to plant, required cooling load and wet-bulb temperature (which is calculated by dry-bulb temperature and relative humidity of air).$T_{\mathrm{cwni,set,L}}$ and $T_{\mathrm{cwni,set,H}}$ are the lower and upper limits set for the cooling water inlet network temperature in a specific time period. In an evaporative cooling tower, since the leaving water temperature is more than wet-bulb temperature, $T_{\mathrm{cwni,\ set,\ L}}$ is defined as follows [56]:

$$T_{\mathrm{cwni,set,L}}=\mathrm{minimum}\left(T_{\mathrm{i}}\in(T_1,\ldots,T_{\mathrm{n}})|T_{\mathrm{i}}\ge T_{\mathrm{wb,L}}\right) \tag{36}$$

If $\left(T_1,\ldots,T_{\mathrm{n}}\right)$ are all possible values for temperature regulation and $T_{\mathrm{wb,L}}$ is the lowest wet-bulb temperature in the specific time period, $T_{\mathrm{cwni,set,H}}$ is set as follows [56]:

$$T_{\mathrm{cwni,set,H}} = \mathrm{maximum}\left(T_1, \ldots, T_n\right) \tag{37}$$

The following equation is used to calculate the wet-bulb temperature [57]:

$$\begin{aligned} T_{\mathrm{wb}} = & T_{\mathrm{a}} \times \arctan\left[0.151977 \times (rh\% + 8.313659)^{1/2}\right] \\ & + \arctan\left(T_{\mathrm{a}} + rh\%\right) - \arctan\left(rh\% - 1.676331\right) \\ & + 0.00391838 \times (rh\%)^{3/2} \times \arctan\left(0.023101 \times rh\%\right) \\ & - 4.686035 \end{aligned} \tag{38}$$

where $T_{\mathrm{a}}$ and rh are dry-bulb temperature and relative humidity of air, respectively. The electrical power consumption of the cooling tower in the ACN is higher than other equipment, so its energy modeling should be designed to consider the effects of changes in inlet air temperature and humidity as shown in Fig. 4. The electrical power consumption of the cooling tower consists of two parts. The first part is related to the fan electrical power consumption, which varies with the temperature set for the inlet cooling water of the ACN, air temperature and humidity and fan efficiency. The second part is related to the electrical power consumption of the cooling tower pump which varies with the flow rate of cooling water and pump efficiency.

Cooling tower energy modeling was conducted based on data-driven models, which are a series of empirical, semi-empirical or fuzzy relationships [58–60].

The empirical relation can be used to model the cooling tower by which the approach temperature is calculated. This model contains 35 coefficients and 4 variables that are given in Appendix.

The cooling tower pump and chilled water pump are used to send water from the cooling tower and storage tank to the ACN, respectively. Variable speed pumps can be used to reduce plant electrical power consumption and adjust the amount of water required by the network.

The mass flow rate of the variable speed pump of cooling tower is calculated according to [62]:

$$\dot{M}_{\mathrm{cwni}} = R_{\mathrm{P}} * \dot{M}_{\mathrm{cwni,rated}} \tag{39}$$

The electrical power consumption of the pump is directly proportional to the flow rate of the pump and its head, and it also is inversely proportional to its efficiency [62]:

$$\dot{W}_{\mathrm{cwp}} = \frac{\left(\dot{M}_{\mathrm{cwni}} \times g \times h_{\mathrm{cwp}}\right)}{\eta_{\mathrm{cwp}}} \quad (\mathrm{kW}) \tag{40}$$

where $\dot{M}_{\mathrm{cwni}}, h_{\mathrm{cwp}}, g$ and $\eta_{\mathrm{cwp}}$ are cooling water flow rate, cooling water pump head, gravity acceleration and cooling water pump efficiency, respectively.

### Scenario of ON and OFF network chillers

In the network where several chillers operate in parallel to supply the plant required cooling load, the optimal condition is to determine which chillers need to be switched on at the same time to fully meet the required cooling load. This can lead to significant energy saving. However, this scenario is most likely to apply when several chillers with different cooling capacities or different types are used in the network. With this scenario, we can determine the optimal thresholds for turning on/off network chillers. Hence, this scenario has divided into two categories: the method of optimal load distribution between chillers and the method of determining the optimal number of chillers [39].

In ACN, the maximum cooling capacity of network increases with decreasing temperature of cooling water lower than design temperature of chillers cooling water and decreases with increasing temperature of cooling water further than design temperature. The maximum cooling capacity $\dot{Q}_{\mathrm{C,max}}$ and the nominal capacity are usually considered equal.

The distribution of the cooling load among the network chillers can be calculated from [63] expressed as:

$$\dot{Q}_{\mathrm{AC,i}} = \frac{\dot{Q}_{\mathrm{C,t}}}{\sum_{i=1}^{N} \dot{Q}_{\mathrm{AC,i,max}}} \times \dot{Q}_{\mathrm{AC,i,max}} \tag{41}$$

where $\dot{Q}_{\mathrm{C,t}}$ and $\dot{Q}_{\mathrm{AC,i,max}}$ are the total cooling load of network and maximum cooling capacity of each absorption chiller in the network, respectively.

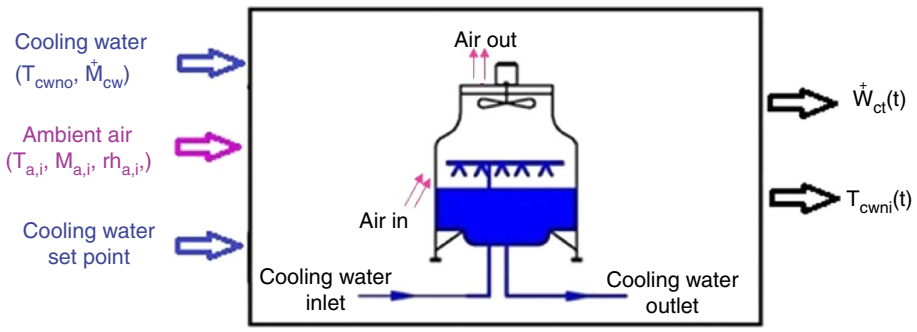


**Fig. 4** The schematic of the model for forced-draft cooling **tower**

Two control methods are widely used to turn on and off cooling towers. In the first method, called "ascendant sequencing control," due to the number of chillers that are ON, the same number of cooling towers is first turned on at the highest speed, and then if the temperature of the cooling water exceeds the upper limit temperature, the number of cooling towers is increased. In the second method, called "descendant sequencing control," unlike the first method, initially all cooling towers were switched on simultaneously regardless of the number of ON chillers, and if the temperature of the output cooling water was lower than the lower limit, the towers will be turned off until the temperature rises to a lower limit temperature. In both methods, the cooling tower fan speed varies between 30 and 100% using the PI controller, depending on the water outlet temperature of the cooling tower [64].

### Scenario of optimizing the network outlet chilled water temperature

The optimization of the chilled water temperature of the ACN outlet is considered as the third scenario. Optimizing the chilled water temperature of the network outlet improves the network efficiency and reduces the fuel and electricity consumption of the plant. Increasing the chilled water temperature of the network outlet reduces fuel and electricity consumption and increases plant efficiency.

To provide the required cooling load, the chilled water temperature of the network outlet must be in accordance with the set temperature for chilled water [56].

$$T_{\text{chwno,set}}^{\text{argmin}}\left(E_{\text{t}}|_{t_0}^{t_0+\Delta t}\right)=\text{minimum}\left(\int_{t_0}^{t_0+\Delta t}\left(\dot{E}_{\text{W}_{\text{ACNP,t}}}(t)\right)\text{d}t+\dot{E}_{\text{Q}_{\text{b}}}(t)\text{d}t\right);\quad t\in\left[t_0,t_0+\Delta t\right] \tag{42}$$

$$T_{\text{chwno,set,L}}\le T_{\text{chwno,set}}\left(t_0\right)\le T_{\text{cwno,set,H}} \tag{43}$$

### Scenario of changing the inlet chilled water, cooling water and steam flow rate

Reducing the flow rate of cooling water and chilled water reduces the power consumption of the cooling pump and chilled pump, respectively. Since the cooling pump and chilled pump have the highest electricity consumption in the ACNP, their optimization improves the $\text{ECOP}_{\text{ACNP}}$ and reduces the $\text{AOC}_{\text{ACNP}}$. To investigate this scenario, because the flow rate change causes the overall heat transfer coefficient (U) to change and U can no longer be assumed constant in computation, using Eqs. (44) to (52) for each case, the U of the respective heat exchanger is calculated. Then, the ACN is analyzed using the flowchart shown in Fig. 2. The equations needed to calculate the U of each absorption chiller exchanger are given below, assuming that the exchangers are clean and no sediment is formed in them.

- Evaporator

The overall heat transfer coefficient for the evaporator exchanger in the absorption chiller is obtained using the following equation [65].

$$U_{\text{EVA}}=\left[\frac{1}{h_{\text{f}}}+\frac{\text{Ln}\left(\frac{D_{\text{o}}}{D_{\text{i}}}\right)}{k}+\frac{\frac{D_{\text{i}}}{D_{\text{o}}}}{h_{\text{eva}}}\right]^{-1} \tag{44}$$

where $h_{\text{f}}, D_{\text{o}}, D_{\text{i}}, k$ and $h_{\text{EVA}}$ are convection heat transfer coefficient of fluid, evaporator tube outer diameter, evaporator tube inner diameter, the thermal conductivity of tube and evaporation heat transfer coefficient, respectively.

The convection heat transfer coefficient $h_{\text{f}}$ is calculated using the Dittus–Bolter formula given below [65].

$$\text{Nu}=0.023\times\text{Re}^{0.8}\text{Pr}^{\text{n}},\ n=0.3\text{ for cooling},\ n=0.4\text{ for heating} \tag{45}$$

$$h_{\text{f}}=\frac{\text{Nu}\times k}{L} \tag{46}$$

where $L$ is the evaporator tube length.

The evaporation heat transfer coefficient $h_{\text{eva}}$ is calculated using the modified Rousseau relation for lower atmospheric pressures using the following equation [66]

$$T_{\text{W}}-T=\left(\frac{C_{\text{sf}}}{C_{\text{Pf}}}\right)\times\left[\frac{q''}{\mu_{\text{l}}h_{\text{fg}}}\sqrt{\frac{\sigma}{\left(\rho_{\text{l}}-\rho_{\text{g}}\right)}}\right]^{\text{n}}\times\left(\frac{P}{P_{\text{atm}}}\right)^{\text{m}}\left(\frac{A_{\text{wetted}}}{A_{\text{base}}}\right)^{\alpha} \tag{47}$$

In the above equation, $T_{\text{W}}, \mu_{\text{l}}, h_{\text{fg}}, \sigma, q'', \rho_{\text{l}}, P_{\text{atm}}, A_{\text{wetted}}$ and $A_{\text{base}}$ are tube wall temperature, liquid viscosity, latent heat of vaporization, surface tension, heat flux, liquid density, atmospheric pressure, wetted area and base area, respectively.

where $C_{\text{sf}}$ and n are 0.0132 and 0.33, respectively. m and α for water boiling at low pressure up to 2 kPa are 0.293 and − 0.0984, respectively.

- Condenser

The overall heat transfer coefficient for the condenser exchanger in the absorption chiller is obtained using the following equation [65].

$$U_{\mathrm{CON}} = \left[ \frac{1}{h_{\mathrm{f}}} + \frac{\mathrm{Ln}\left(\frac{D_{\mathrm{o}}}{D_{\mathrm{i}}}\right)}{k} + \frac{\frac{D_{\mathrm{i}}}{D_{\mathrm{o}}}}{h_{\mathrm{CON}}} \right]^{-1} \tag{48}$$

where $h_{\mathrm{f}}, D_{\mathrm{o}}, D_{\mathrm{i}}, k$ and $h_{\mathrm{CON}}$ are convection heat transfer coefficient of fluid, condenser tube outer diameter, condenser tube inner diameter, the thermal conductivity of tube and condensation heat transfer coefficient, respectively. The convection heat transfer coefficient $h_{\mathrm{f}}$ is calculated using the Dittus–Bolter formula. The condensation heat transfer coefficient of $h_{\mathrm{CON}}$ is calculated using the Adams condensation relation given below [65]

$$h_{\mathrm{CON}} = 1.13\left(\frac{k_{\mathrm{f}}^3 \rho_{\mathrm{f}}^2 g}{\mu_{\mathrm{f}}}\right)^{0.25} \times \left(\frac{h_{\mathrm{fg}}}{L\Delta T}\right) \tag{49}$$

where $k_{\mathrm{f}}$, $\rho_{\mathrm{f}}$, $\mu_{\mathrm{f}}$, $L$ and $\Delta T$ are thermal conductivity, density, dynamic viscosity, length of condenser tube and temperature difference, respectively.

- Absorber

The overall heat transfer coefficient for the absorber exchanger in the absorption chiller is obtained using the following equation [65].

$$U_{\mathrm{ABS}} = \left[ \frac{1}{h_{\mathrm{f}}} + \frac{\mathrm{Ln}\left(\frac{D_{\mathrm{o}}}{D_{\mathrm{i}}}\right)}{k} + \frac{\frac{D_{\mathrm{i}}}{D_{\mathrm{o}}}}{h_{\mathrm{sol}}} \right]^{-1} \tag{50}$$

where $\mathrm{h_f}, \mathrm{D_o}, \mathrm{D_i}$, k and $\mathrm{h_{sol}}$ are convection heat transfer coefficient of fluid, absorber tube outer diameter, absorber tube inner diameter, the thermal conductivity of tube and solution heat transfer coefficient, respectively. The convection heat transfer coefficient $h_f$ is calculated using the Dittus–Bolter formula. The convection heat transfer coefficient of the solution $h_{\mathrm{sol}}$ is calculated using the following equation [67].

$$h_{\mathrm{sol}} = \frac{k_{\mathrm{sol}}}{\delta}\left[0.029\left(\frac{4.\Gamma}{\mu}\right)^{0.53} \mathrm{Pr}_{\mathrm{sol}}^{0.344}\right] \tag{51}$$

where $\delta$ and $\Gamma$ are solution film thickness and mass flow rate, respectively.

- Generator

The overall heat transfer coefficient for the generator exchanger in the absorption chiller is obtained using the following equation [65].

$$U_{\mathrm{GEN}} = \left[ \frac{1}{h_{\mathrm{f}}} + \frac{\mathrm{Ln}\left(\frac{D_{\mathrm{o}}}{D_{\mathrm{i}}}\right)}{k} + \frac{\frac{D_{\mathrm{i}}}{D_{\mathrm{o}}}}{h_{\mathrm{sol}}} \right]^{-1} \tag{52}$$

where $h_{\mathrm{f}}, D_{\mathrm{o}}, D_{\mathrm{i}}, k$ and $h_{\mathrm{sol}}$ are convection heat transfer coefficient of fluid, generator tube outer diameter, generator tube inner diameter, the thermal conductivity of tube and solution heat transfer coefficient, respectively. The convection heat transfer coefficient $h_{\mathrm{f}}$ is calculated using the Dittus–Bolter formula given above.

#### Combination of prior scenarios

In this scenario, considering the first, second, third and fourth scenarios together, it was seeking to improve the $\mathrm{ECOP_{ACN}}$ and reduce the $\mathrm{AOC_{ACNP}}$.

## Optimization method applied

As a part of the optimization processes, it was necessary to select the objectives functions, the decision variables and constraints to achieve the best configuration to the ACNP.

#### Objective Functions, Decision variables and Constraints

Two objective functions are considered in the one-objective optimization, which are "maximizing the $\mathrm{ECOP_{ACN}}$" as a thermodynamic criterion and "minimizing the $\mathrm{AOC_{ACNP}}$" as an economic criterion. The optimization process was performed separately for each of the mentioned objective functions, using the particle swarm optimization search algorithm. In the case of two-objective optimization, the optimal values of both objective functions are reported simultaneously by using the multi-objective particle swarm optimization (MOPSO) search algorithm.

The five decision variables considered in the present study are:

- Cooling water inlet temperature of network ($T_{\mathrm{cwni}}$)
- Solution heat exchanger efficiency $\left(\eta_{\mathrm{SHX}}\right)$
- Opening percentage of inlet steam control valve $\left(\mathrm{CV_{stni}}\right)$
- Inlet steam temperature of network $\left(T_{\mathrm{stni}}\right)$
- Chilled water outlet temperature of network $\left(T_{\mathrm{chwno}}\right)$

The decision variables considered except the heat exchanger efficiency are all operational variables and can be achieved by choosing the optimal conditions. The variation ranges of the above variables are optimization constraints as follows:

$$25\,^{\circ}\mathrm{C} \le T_{\mathrm{cwni}} \le 38\,^{\circ}\mathrm{C} \tag{53}$$

$$0.2 \le \eta_{SHX} \le 0.7 \quad (54)$$

$$40\% \le CV_{stni} \le 100\% \quad (55)$$

$$120\,^{\circ}C \le T_{cwni} \le 150\,^{\circ}C \quad (56)$$

$$10\,^{\circ}C \le T_{chwno} \le 11\,^{\circ}C. \quad (57)$$

### One-objective optimization search algorithm

In this research, the use of the particle swarm optimization (PSO) algorithm significantly increased the response speed and provided a response with high accuracy. Figure 5 depicts the flowchart of this type of optimization. Table 5 presents the values of the parameters of this method for writing computer code on MATLAB [68].

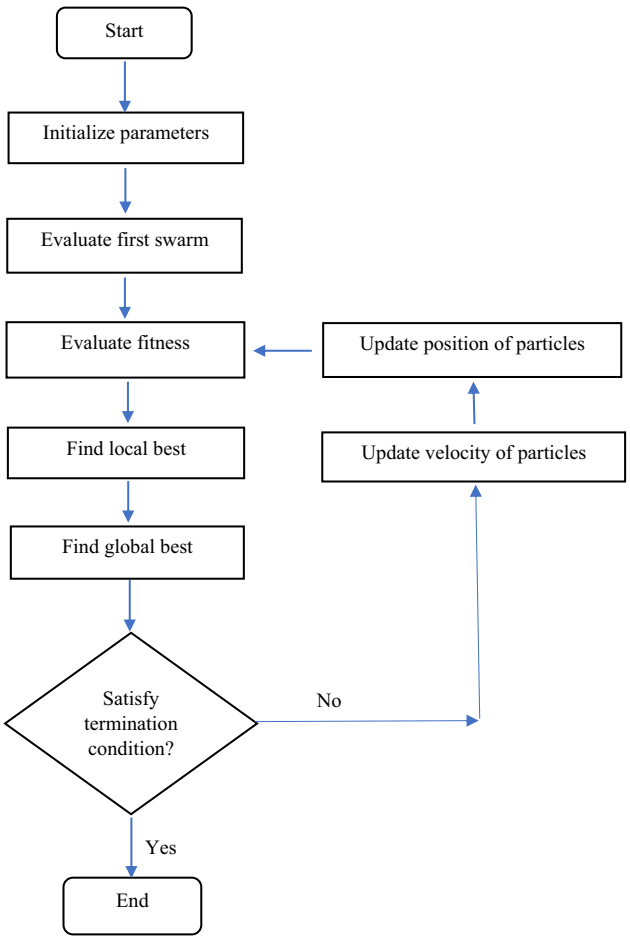


**Fig. 5** PSO optimization flowchart

**Table 5** Parameters used for the optimization on MATLAB for PSO algorithm

| Parameter | Value |
|---|---|
| Function tolerance | $10^{-4}$ |
| Inertia range | 0.1-1.2 |
| Initial swarm span | 1800 |
| Max stall iterations | 250 |
| Self and social adjustment weights | 1.12 |
| Swarm size | 50 |

### Two-objective optimization search algorithm

MOPSO search algorithm is used for the two-objective optimization. The parameter values of this method are given in Table 6.

To perform the optimization using the search algorithms mentioned (PSO) and (MOPSO), it was necessary to link the EES software to MATLAB software and then obtain the optimal values of the objective functions using the computer code written in MATLAB.

### Decision-making method

In the multi-objective optimization, a set of optimal solutions is obtained for each objective function and plotted on a plane diagram (Pareto curve). In this curve, a point is considered as the ideal answer, in which both goals are satisfied regardless of the other points. It should be noted that this point is hypothetical and is not on the Pareto curve. On the other hand, in many cases, the objective functions defined in the multi-objective optimization problem are at odds with each other. In such a case, it is said that for a multi-objective optimization problem, there will be Pareto optimal solutions (theoretically, there may be many Pareto optimal solutions for multi-objective optimization problem) [69–72].

Accordingly, decision-making methods should be used to find the optimal solution from the set of Pareto optimal

**Table 6** Parameters used for the optimization on MATLAB for MOPSO algorithm

| Parameter | Value |
|---|---|
| Population size | 100 |
| Repository size | 200 |
| Maximum number of generations | 100 |
| Inertia weight | 0.4 |
| Individual confidence factor | 1.75 |
| Swarm confidence factor | 1.8 |
| Number of grids in each dimension | 20 |
| Maximum velocity in percentage | 5 |
| Uniform mutation percentage | 0.5 |

solutions obtained from the search algorithm [73]. So far, researchers have proposed various decision-making methods such as Bellman and Zadeh [74] and LINMAP and TOPSIS [75, 76], which should be normalized so that they can be used in the process [77].

There are two important points in the Pareto curve: one of which is a positive ideal solution (PIS) and the second one is a negative ideal solution (NIS). To select the best solution, the LINMAP decision-making method only considers one point that is the closest point to the positive ideal solution (PIS). However, the TOPSIS method not only considers the shortest distance to the PIS point but also uses the farthest point from the negative ideal solution (NIS) [78].

In this study, the $ECOP_{ACN}$ and the $AOC_{ACNP}$ were linear normalized, expressed them as:

$$ECOP^{*}_{ACN} = \frac{ECOP_{ACN} - ECOP_{ACN,min}}{ECOP_{ACN,max} - ECOP_{ACN,min}} \tag{58}$$

$$AOC^{*}_{ACNP} = \frac{AOC_{ACNP} - AOC_{ACNP,min}}{AOC_{ACNP,max} - AOC_{ACNP,min}} \tag{59}$$

The LINMAP method was used to select the optimal solution, in which the ideal solution was the best solution and the Euclidean distance of each point on the Pareto frontier curve was calculated as [71–73]:

$$D_{i+} = \sqrt{\sum_{j=1}^{m}(F_{ij} - F_{j}^{ideal})^2} \tag{60}$$

where $F_{j}^{ideal}$ represents the optimal value of the function j, m indicates the number of objective functions, i shows the solutions on the Pareto frontier graph, and $i_{final}$ is the final solution chosen by this method and is calculated by the following equation [71–73]:

$$i_{final} = i\varepsilon\min\left(D_{i+}\right) \tag{61}$$

Figure 6 shows the proposed optimization method for the ACNP in the present study. As can be seen first, the decision variables, constraints, objective functions, values of the MOPSO search algorithm parameters and the initial guess for thermodynamic variables are specified. For each component of the plant, calculations are performed in EES and the amount of specified output variables is determined. After verifying the results by checking the mass and energy balance for the ACNP's components, the values of objective functions in MATLAB are calculated for each generation of MOPSO. Then, the optimal values of each generation are put in the optimal matrix. After that, the number of generations is checked and if exceeds the specified value, the Pareto curve is plotted by using the optimal values in the matrix and applied the LINMAP decision-making method to choose the best optimal solution. Finally, the optimal operating conditions of the plant are proposed according to the best optimal solution obtained.

## Marun Petrochemical Company's ACNP - Case study

To verify the capability of the model, the presented analysis was applied to the Marun petrochemical company (M.P.C.) ACNP. This section first describes the case study and then reports the validation of numerical modeling results and sensitivity analysis. At last, this section discusses the results of thermodynamic and economic analysis and optimization methods.

### Description of the case study ACNP

The absorption chiller network plant simulated and analyzed in this study is absorption chillers that composed the Mono-Ethylene Glycol - MEG Production Plant, in Fig. 7, of the Marun petrochemical company located in Iran. This plant consists of four single-effect steam absorption chillers, two forced-draft cooling towers, a chilled water pump device, a chilled water storage tank, two heat exchangers and two cooling towers' water pumps. The performance of the aforementioned ACNP is such that chilled water in two heat exchangers (HX200 and HX300) absorbs heat from process fluid and collects them in the chilled water storage tank. The chilled water from the storage tank is sucked by the chilled water pump and is distributed simultaneously between four absorption chillers (same cooling capacity of 4775 kW) in the parallel arrangement. After cooling, the chilled water is sent back to the heat exchangers. The cooling water is cooled in forced-draft fan cooling towers sucked by cooling pumps and is sent to the absorber and condenser of chillers.

The operating data of the concerned ACN on June $10^{th}$, 2017, were measured with an infrared thermometer (uncertainty $\pm 0.1$); ultrasonic mass flow meter (uncertainty $\pm 2.2$) and a digital multimeter (uncertainty $\pm 1$) are listed in Table 7. The total required cooling load of heat exchangers was assumed to be constant and equal to 19,100 kW.

### Economic inputs of the case study ACNP

The ACNP investment cost is calculated based on the values taking from Table 4 and Eq. (27) shown in Table 8. Since we assumed this case study used existing steam, the cost of boiler investment has been neglected. In the considered ACNP, we assumed all the chillers work with the steam produced in the MEG distillation column, because the steam produced in the MEG distillation column is not waste steam and can be used in other applications in the petrochemical

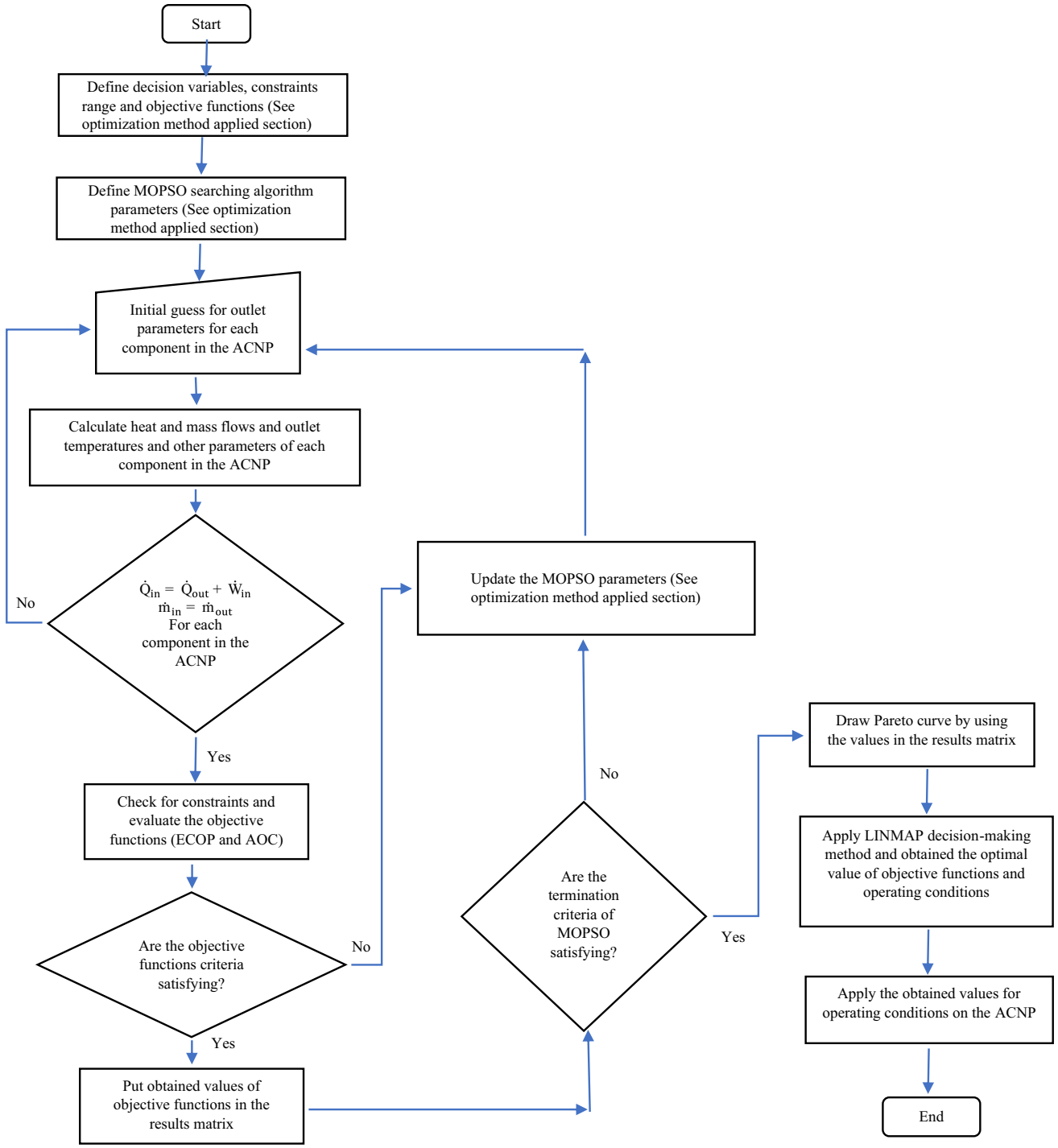


**Fig. 6** The ACNP proposed optimization

complex. In the present study, the value of this steam was calculated using the following formula [82].

$$S_C = \frac{\text{Fuel Cost} \times \left(h_{\text{Steam}} - h_{\text{Feed water}}\right)}{1000 \times \eta_b} \tag{62}$$

where the heat value of the fuel is in \$ $MJ^{-1}$ and the enthalpy of steam and feed water is in kJ $Kg^{-1}$ and $\eta_b$ is also the boiler efficiency. The cost of consuming steam of plant is calculated in dollars per year as follows.

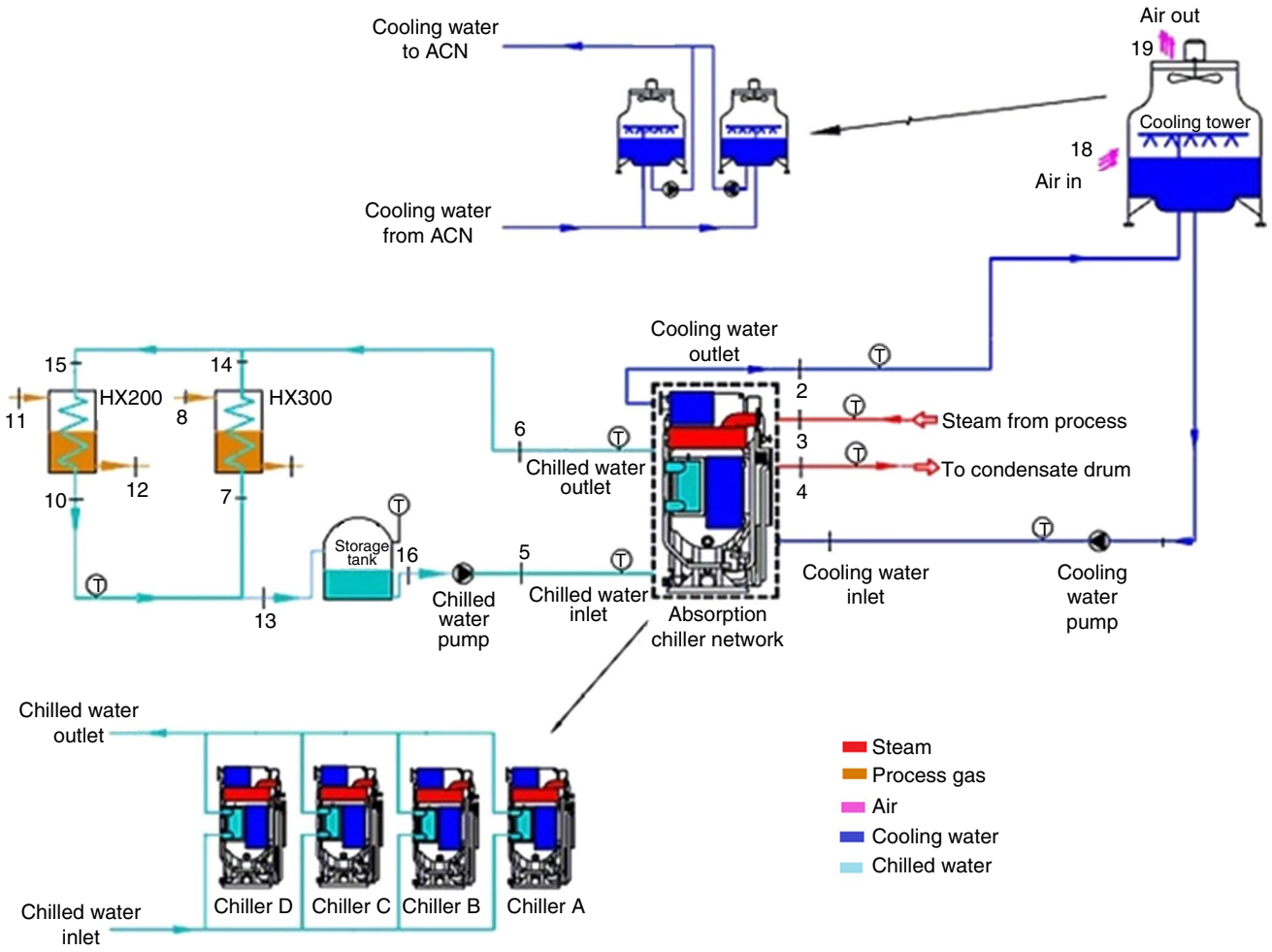


**Fig. 7** Schematic of the ACNP: case study

**Table 7** Data measured on the site

| Parameter | Value | Unit | Parameter | Value | Unit |
|---|---|---|---|---|---|
| The chilled water inlet temperature | 16.8 | °C | Steam outlet temperature (generator) | 95 | °C |
| The chilled water outlet temperature | 10.2 | °C | Steam flow rate | 12 | Kg $s^{-1}$ |
| Chilled water flow rate | 672 | Kg $s^{-1}$ | Airflow rate of each cooling tower | 520 | $m^3$ $s^{-1}$ |
| Ambient temperature | 43.5 | °C | Each cooling tower fan power consumption | 90 | kW |
| Cooling water inlet temperature (absorber) | 35 | °C | Each cooling tower pump power consumption | 485 | kW |
| Cooling water outlet temperature (condenser) | 43 | °C | Chilled water pump power consumption | 216 | kW |
| Cooling water flow rate | 1398 | Kg $s^{-1}$ | Steam condensate pump power consumption | 3.7 | kW |
| Steam inlet temperature (generator) | 145 | °C | Each absorption chiller pump power consumption | 8.9 | kW |

$$C_S = S_C \times \dot{m}_S \times 3600 \times t_{year}$$
$$C_{invs} = 2{,}898{,}584.873\$ \tag{63}$$

$C_{invs} = 2{,}898{,}584.873$ $

The plant repair cost is 6% of the investment cost [1]. The plant lifetime is 20 years for the ACNP [79]. The price of natural gas is 0.843 ($ $GJ^{-1}$) [80], the purchase price of electricity is 0.06 ($ $kWh^{-1}$) [53], and the plant operating hour is 7000 (hours $year^{-1}$).

**Table 8** Investment cost of ACNP

| Component | Cost/$ |
|---|---|
| Evaporators | 794952.274 |
| Absorbers | 861990.900 |
| Generators | 305453.215 |
| Solution HX | 267372.501 |
| Condensers | 372340.812 |
| Cooling Towers | 205585.964 |
| Pump cooling towers | 62155.612 |
| pump chilled water | 28733.595 |
| Total | 2898584.873 |

**Table 9** Comparison of numerical modeling results with measured experimental values for outlet chilled water temperature of the network ($T_{chwni}$ = 16.8 °C and $T_{stni}$ = 145 °C)

| Tcwno/ °C | Num./ °C | Exp./ °C | Diff./ % |
|---|---|---|---|
| 32 | 9.42 | 9.3 | 1.27 |
| 33 | 9.66 | 9.7 | 0.4 |
| 34 | 9.78 | 9.9 | 1.2 |
| 35 | 10.06 | 10.2 | 1.37 |
| 36 | 10.12 | 10.6 | 4.53 |
| 37 | 10.24 | 10.8 | 5.19 |
| 38 | 10.48 | 11 | 4.73 |

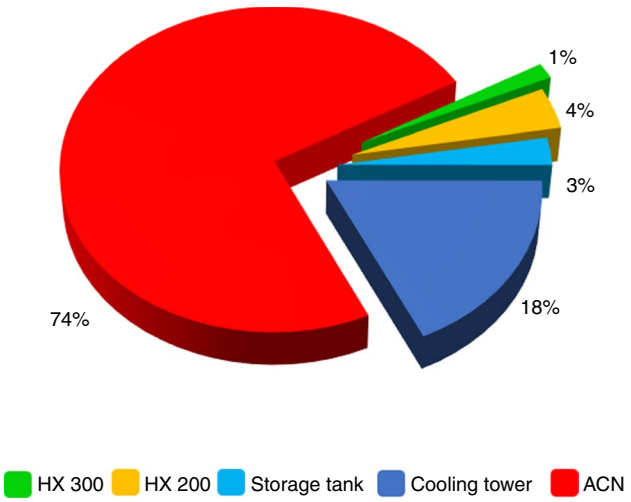


**Fig. 8** Exergy destruction percentage in components of ACNP

## Validation of numerical modeling results

In Table 9, the results calculated using the numerical code for the outlet chilled water temperature of the chiller network were compared with the experimental temperature measured at the site while the temperature of cooling water was variable.

As can be seen in Table 9, the highest relative error between the numerical and experimental results was around 5% and the lowest one was less than 1%., which proves that the developed model was accurate.

# Results and discussion

## Energy and exergy analysis results of ACNP

The exergy destruction percentage in components of ACNP is shown in Fig. 8. The ACN has the highest exergy destruction rate under operating conditions. The cooling tower also has a second position. The total exergy destruction of the chilled water storage tank and heat exchangers is less than 10%.

Figure 9 depicts the exergy flows and the exergy destruction rate of the main components of the ACN. As shown, the absorbers and evaporators have the highest exergy loss among the absorption chiller components of the network due to more entropy generated in them. Phase change phenomena of refrigerant which happened in evaporators and absorption process of concentrated $LiBr/H_2o$ solution in absorbers inherently cause significant entropy generation and endogenous avoidable exergy destruction in these components which can be reduced by improving the design of them and selecting the optimum operating conditions.

## Parametric analysis of ACNP

A parametric examination was undertaken to verify the behavior of systems taking into account the temperatures, such as the generator solution temperature, network chilled water outlet temperature, outlet chilled water temperature, solution concentration of generator outlet of ACN, outlet chilled water temperature and outlet cooling water temperature of ACN, and also energy–exergy parameters such as COP, ECOP, exergy input, and exergy destruction of ACN, exergy destruction of network chillers absorber, exergy destruction percentage in the absorber, generator and evaporator of ACN.

To complete the examination, we selected several variables to investigate the influence of the quality of chiller output steam, the inlet steam flow rate, the inlet cooling water temperature, the flow rate of the chiller solution pump and the solution heat exchanger efficiency on the temperatures and energy–exergy parameters of the system. Tables 10, 11, and 12 show the variables keeping constant along of the simulation of each case.

**Case a** The behavior of the systems varies the steam inlet network flow rate and temperature, the quality of condensate steam outlet and solution pump flow rate

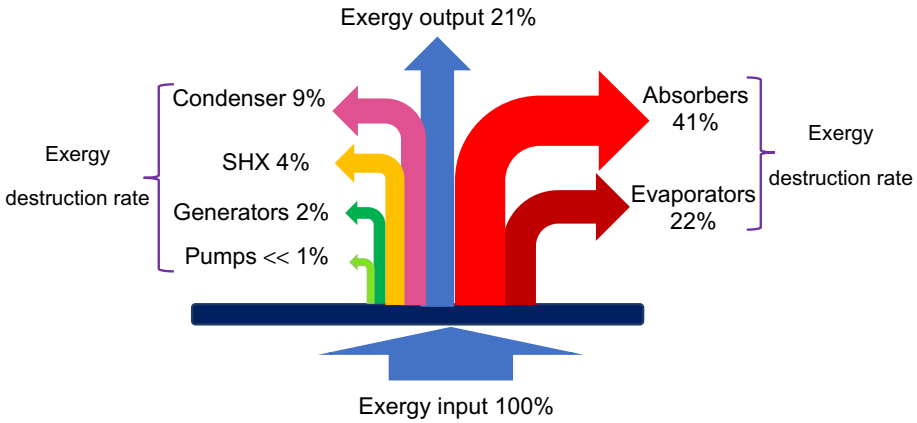


**Fig. 9** Exergy flow diagram of ACN

**Table 10** The variable keeping constant for case a

| Cooling water inlet network ($T_{cwni}$) | Steam inlet network ($T_{stni}$) | Chilled water inlet network ($T_{chwni}$) | Solution heat exchanger efficiency ($\eta_{SHX}$) |
|---|---|---|---|
| 35 °C | 145 °C | 16.8 °C | 0.6 |

The graphics of Fig. 10a show the behavior of exergy destruction in the absorber, $ECOP_{ACN}$, generator solution temperature, and network chilled water outlet temperature by changing the quality of chiller output condensate steam, and Fig. 10b shows the behavior of COP, ECOP, exergy input and exergy destruction of ACN with inlet steam flow rate. Table 10 shows the variables keeping constant for the case a.

As observed in Fig. 10a, a decrease in the steam quality of the generator output results in a higher $ECOP_{ACN}$ and absorber exergy destruction. In addition, any decrease in the output steam quality increases the amount of heat transferred to the generator solution. Therefore, according to the energy balance in the chiller, this process raises the amount of heat taken from steam, increases the generator solution temperature ($T_4$) and reduces the network chilled water outlet temperature.

As shown in Fig. 10b, an increase in the percentage of steam input to the ACN in the design mode from 50 to 100% slightly increases $COP_{ACN}$, due to the lower chilled water temperature of the network outlet and increased heat transfer in the evaporator of chillers in the network. When $COP_{ACN}$ reaches 67.55% by increasing the amount of steam entering the network, a slight decrease is observed in $COP_{ACN}$ due to a further increase in heat transfer in the generator compared to the evaporator of chillers in the network. Moreover, as illustrated in Fig. 10b, an increase in the percentage of steam input to the network caused a decrease in the ratio of exergy destruction to exergy input and increased the $ECOP_{ACN}$.

As shown in Fig. 11a, changes in solution pump flow rate first increase and then decrease $COP_{ACN}$ while a reverse trend is observed in the chilled water temperature. Decreasing the solution pump flow rate increases the solution concentration. Compared to the design mode, a decrease in flow rate by more than 30% increases the solution concentration

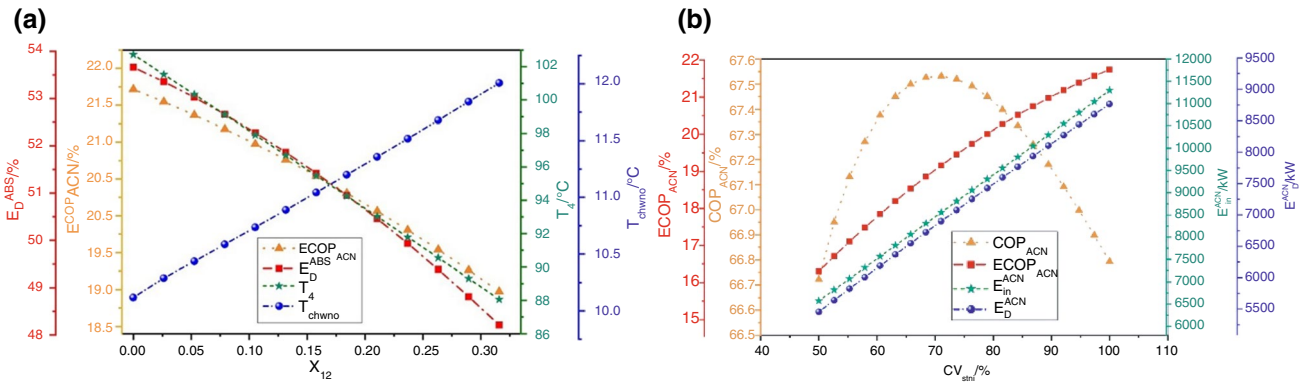


**Fig. 10** **a** The behavior of exergy destruction in the absorber, $ECOP_{ACN}$, generator solution temperature and network chilled water outlet temperature by changing the quality of chiller output steam. **b** The behavior of COP, ECOP, exergy input and exergy destruction of ACN with inlet steam flow rate

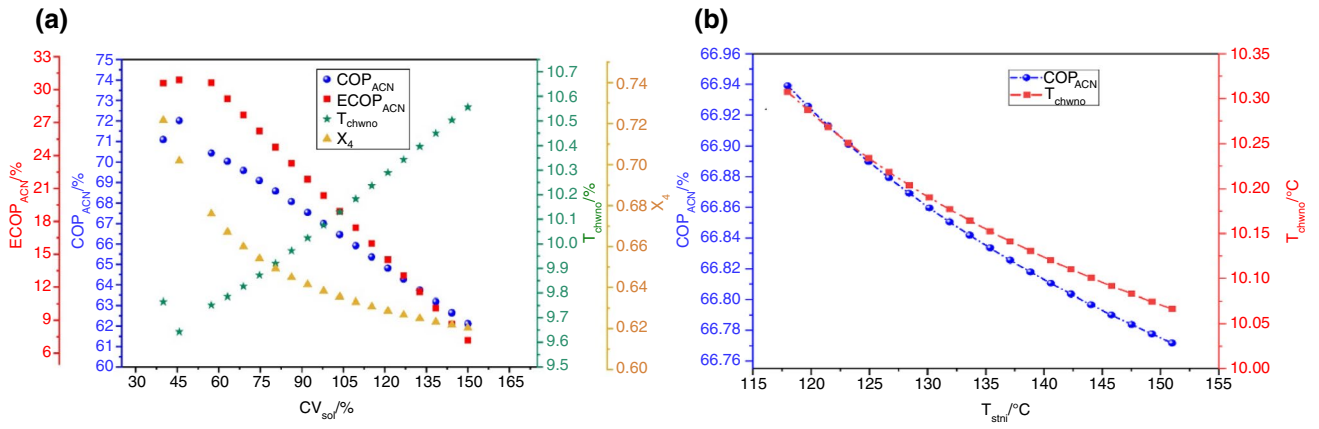


**Fig. 11** **a** The behavior of ECOP, COP, outlet chilled water temperature and solution concentration of generator outlet of ACN by changing the flow rate of the chiller solution pump. **b** The behavior of outlet chilled water temperature and COP with network inlet steam temperature

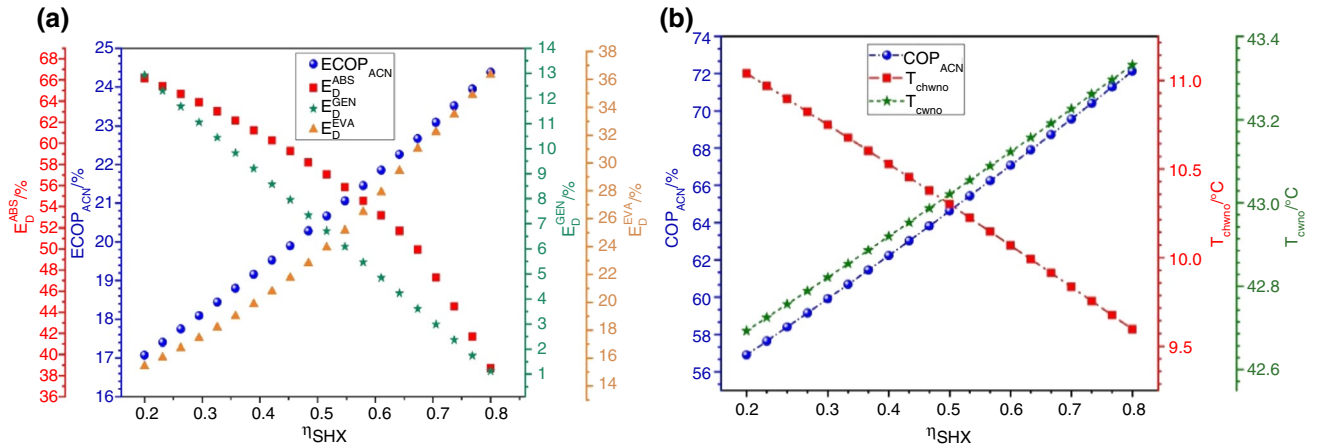


**Fig. 12** **a** The behavior of ECOP, exergy destruction percentage in the absorber, generator and evaporator of ACN with solution heat exchanger efficiency. **b** The behavior of COP, outlet chilled water temperature and outlet cooling water temperature of ACN with solution heat exchanger efficiency

by more than 65 mass% and causes its crystallization. On the other hand, increasing solution pump flow rate increases total exergy destruction and decreases $ECOP_{ACN}$, due to increased exergy destruction in absorber and generator of network chillers. Figure 11b demonstrates the variation of the outlet chilled water temperature and $COP_{ACN}$ with network inlet steam temperature. As observed, an increase in the network inlet steam temperature increases the heat transfer rate in the chillers generator and leads to the higher separation of the refrigerant from $LiBr/H_2O$ solution and higher generator pressure. These two factors cause more refrigerant to be condensed in the condenser and sent to the chiller evaporator for spraying, which reduces the outlet chilled water temperature of the network. Furthermore, an increase in the inlet steam temperature increases the heat transfer rate in the evaporator and generator simultaneously, although the heat transfer rate in the generator is slightly higher than that of the evaporator. According to Eq. (1), the $COP_{ACN}$ decreases slowly by increasing steam temperature.

**Table 11** The variable keeping constant for case b

| Cooling water inlet network ($T_{cwni}$) | Steam inlet network ($T_{stni}$) | Chilled water inlet network ($T_{chwni}$) |
|---|---|---|
| 35 °C | 145 °C | 16.8 °C |

**Case b** The behavior of the systems varying the solution heat exchanger efficiency.

The graphics of Fig. 12a show the behavior of ECOP, exergy destruction percentage in the absorber, generator and evaporator of ACN with solution heat exchanger efficiency. Figure 12b shows the behavior of COP, outlet chilled water

temperature and outlet cooling water temperature of ACN with solution heat exchanger efficiency. Table 11 shows the variables keeping constant for the case b.

As shown in Fig. 12a, increasing the efficiency of the solution heat exchanger increases the $ECOP_{ACN}$ and the exergy destruction in the evaporator and decreases the exergy destruction in the absorber and generator. Additionally, an increase in the efficiency of solution heat exchanger increases heat transfer in it, resulting in increasing the dilute solution temperature and decreasing the concentrate solution temperature too which reduced exergy destruction. An increase in the dilute solution temperature of the generator inlet increases the pressure in the generator/condenser shell and decreases the concentrate solution temperature of the absorber inlet. Due to that, more refrigerant moves from the condenser to the evaporator and causes more refrigerant spraying in the evaporator. Accordingly, this increases the exergy destruction of the evaporator and a decrease in the outlet chilled water temperature of the chillers. Figure 12b shows the variations of $COP_{ACN}$, outlet chilled water temperature and outlet cooling water of ACN in terms of the efficiency of the solution heat exchanger. As observed, increasing the efficiency of the solution heat exchanger increases the $COP_{ACN}$ and outlet temperature of the cooling water and decreases the chilled water temperature of the outlet network.

**Case c** The behavior of the systems varies the cooling water inlet network temperature and switching on/off chillers.

The graphics of Fig. 13a show the behavior of $COP_{ACN}$ and outlet chilled water temperature of the network with the inlet cooling water temperature. Figure 13b shows the behavior of ECOP and exergy destruction of network chillers absorber with inlet cooling water temperature. Figure 13c shows the behavior of $COP_{ACN}$ and outlet chilled water temperature of ACN with inlet cooling water temperature for three ON chillers. Table 12 depicts the variables keeping constant for the case c.

**Table 12** The variable keeping constant for case c

| Steam inlet network ($T_{stni}$) | Chilled water inlet network ($T_{chwni}$) | Solution Heat Exchanger Efficiency ($\eta_{SHX}$) |
|---|---|---|
| 145 °C | 16.8 °C | 0.6 |

Figure 13a provides the variation of the COP and outlet chilled water temperature to the inlet cooling water temperature of the network. As shown, decreasing the cooling water temperature decreases the network outlet chilled water temperature and increases its COP. Further, decreasing the network cooling water temperature increases the surface tension gradients at the $LiBr/H_2O$ solution interface and refrigerant vapors, leading to an increased Marangoni effect. Consequently, an increase in the Marangoni effect at the interface between the two phases of liquid and vapor increases the rate of heat and mass transfer processes between the phases. Therefore, decreasing the temperature of the cooling water leads to increased refrigerant vapors absorption and decreased concentration of the solution. On the other hand, a decreased temperature reduces the pressure of the absorber/evaporator shell, which reduces the saturation temperature of the refrigerant in the evaporator and increases the refrigerant vapors production. Both cause the $LiBr/H_2O$ solution to transfer more refrigerant from the absorber to the generator, where more refrigerant is removed from the solution and sent to the condenser. The cooling water enters the condenser from the absorber outlet, leading to the condensation of more refrigerant vapors. Therefore, more refrigerant is sent from the condenser to the evaporator for spraying, which reduces the chilled water temperature of the evaporator outlet. Since the heat transfer in the evaporator is more sensitive to the temperature changes in the cooling water

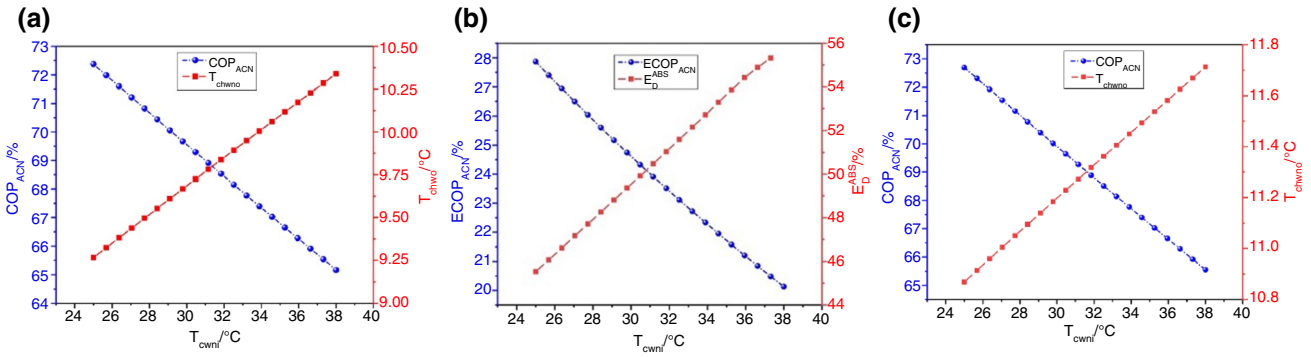


**Fig. 13** **a** The behavior of COP and outlet chilled water temperature of network with the inlet cooling water temperature. **b** The behavior of ECOP and exergy destruction of network chillers absorber with inlet cooling water temperature. c) The behavior of COP and outlet chilled water temperature of ACN with inlet cooling water temperature for three ON chillers

than the heat transfer in the generator, a decrease in the cooling water temperature increases the $COP_{ACN}$ significantly, according to Eq. (1).

As shown in Fig. 13b, decreasing the cooling water temperature increases the $ECOP_{ACN}$, due to the reduced exergy destruction of various exchangers same as the absorber of network chillers. It can be said that a decrease in cooling water temperature leads to the separation of more refrigerant liquid from the solution in the chiller generator, and as a result, more heat is needed in the generator to separate this refrigerant from the solution. Thus, when the chilled water temperature of the network outlet is not set to a specific value, decreasing cooling water temperature increases the total heat transfer rate of the network chillers generator. If the network outlet chilled water is set to the specific temperature, the total heat transfer rate of the generator will decrease by reaching the set point temperature.

By comparing Fig. 13a with Fig. 11b, it can be found that the sensitivity of the network outlet chilled water temperature and $COP_{ACN}$ to the inlet cooling water temperature is higher than that of the network inlet steam temperature. As observed, decreasing the cooling temperature by 13 °C reduces the network outlet chilled water temperature by 1.1 °C, while an increase in the network inlet steam temperature by 26 °C decreases the network outlet chilled water temperature by 0.23 °C. It can be concluded that since the latent energy of steam is mainly used in the vapor-to-liquid phase change process in the network chillers generator, its sensitivity to temperature variation is less than the sensitivity of the condenser and absorber to the variation of their inlet cooling tower water temperature. Thus, this result highlights the higher importance of the precise control of the cooling water temperature in the ACN compared to the steam temperature. Figure 13c presents the variations of $COP_{ACN}$ and network outlet chilled water temperature by changing the cooling water temperature, in which the chilled water and inlet steam temperature are constant and one of the network chillers is switched off. As can be seen, like the four-chiller network, increasing the cooling tower water temperature rises the outlet chilled water temperature and decreases the $COP_{ACN}$ significantly.

Figure 14 shows different curves to illustrate the behavior of the economic variables against energetic indexes; a) $AOC_{ACNP}$, consumption steam cost ($C_S$), $ECOP_{ACN}$, and network outlet chilled water temperature with cooling water inlet network b) $AOC_{ACNP}$, consumption steam cost, $ECOP_{ACN}$ and difference of $LiBr/H_2O$ solution concentration with network outlet chilled water temperature. Figure 15 depicts the behavior of $AOC_{ACNP}$, $COP_{ACN}$, and $ECOP_{ACN}$ against the chiller solution heat exchanger efficiency ($\eta_{SHX}$). The values from Table 12 are used in the modeling of Figs. 14 and 15.

As observed in Fig. 14a, an increase in the temperature of the network inlet cooling water decreases the $ECOP_{ACN}$, because of increasing exergy destruction. Since the outlet chilled water temperature is set to 10 °C, increasing the cooling water temperature first increases the amount of steam

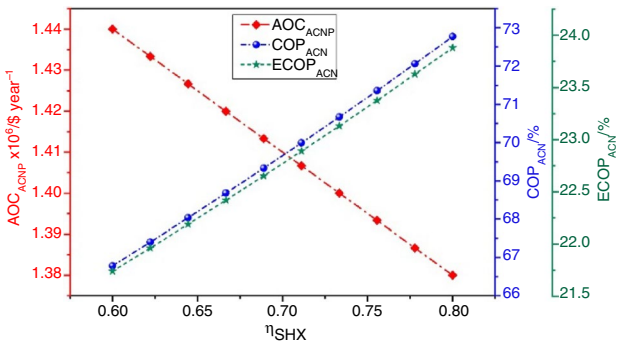


**Fig. 15** The behavior of $AOC_{ACNP}$, $COP_{ACN}$, and $ECOP_{ACN}$ against $\eta_{SHX}$

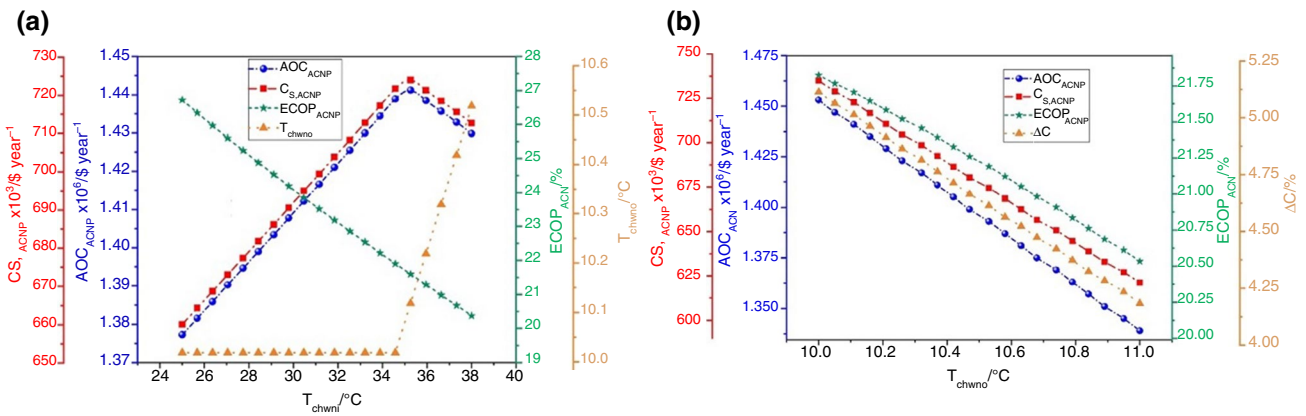


**Fig. 14** The behavior of the economic variables **a** $AOC_{ACNP}$, $C_{S,ACNP}$, $ECOP_{ACN}$, and $T_{chwno}$ with $T_{cwni}$ **b** $AOC_{ACNP}$, $C_{S,ACNP}$, $ECOP_{ACN}$ and solution concentration difference with $T_{chwno}$

consumed by the network chillers to maintain the chilled water temperature at the set temperature. However, when the inlet cooling water temperature rises above 35 °C due to an increase in the LiBr/$H_2O$ solution concentration and the possibility of its crystallization, the inlet network steam decreases. Therefore, the network outlet chilled water temperature increases to more than the set value. As shown, increasing the consuming steam due to the raised temperature of the inlet cooling water increases the $AOC_{ACNP}$ from $1.375\times10^6$ to $1.445\times10^6$ \$ year$^{-1}$.

As shown in Fig. 14b, an increase in the network outlet chilled water temperature reduces the $AOC_{ACNP}$ and decreases the steam consumption, due to the reduced cooling capacity required in the process. In other words, an increase in the outlet chilled water temperature from 10 to 11 °C decreases the solution concentration difference between the generator (maximum concentration) and the absorber (minimum concentration) from 5.125 to 4.125%, as shown in Fig. 14b. On the other hand, increasing the exergy destruction rate to the total input exergy decreases the $ECOP_{ACN}$ from 21.75 to 20.5%. Also, the $AOC_{ACNP}$ reduces from $1.445\times10^6$ to $1.338\times10^6$ \$ year$^{-1}$, due to decreased fuel consumption.

As observed in Fig. 15, increasing the solution heat exchanger efficiency increases the $COP_{ACN}$ and $ECOP_{ACN}$ and decreases $AOC_{ACNP}$ from $1.441\times10^6$ to $1.381\times10^6$ \$ year$^{-1}$, due to decreased exergy destruction and fuel consumption

## Optimization results applied in the system

This subsection is linked to the results of the application of optimization techniques in the studied system. Initially, the results obtained considering the one-objective and two-objective techniques were presented. Finally, the specific results of the scenarios are selected from the system, according to the parameters described in the optimization section.

### One-objective optimization results

The results of one-objective optimization are represented in this section. The results of this section are important because it obtains the optimal value of each objective function individually and, according to it, is possible to propose the operating conditions optimally. Table 13 shows the range of decision variables and their optimal values in ACNP.

For case I, the maximum $ECOP_{ACN}$ is 31.46%, while the inlet cooling water temperature, inlet steam temperature and network outlet chilled water temperature are near the lower limit of their operating range. Ultimately, the heat exchanger efficiency is near the upper limit. For case II, the minimum $AOC_{ACNP}$ is $1.303\times10^6$ \$ year$^{-1}$, while the inlet cooling water temperature is near the lower limit of its operating range. Accordingly, the heat exchanger efficiency, the inlet steam temperature and the network outlet chilled water temperature are near the upper limit, and the network inlet steam flow rate is near the middle of lower and upper limits. In other words, as shown in case I, the minimum cooling water temperature and maximum steam, chilled water temperature and the solution heat exchanger efficiency can be met the economic criterion. Since if only the economic criterion is considered, it will be realized that it is not desirable because the performance of the ACNP under such conditions significantly reduces its useful life and from this point of view, one-objective optimization cannot be effective, it is necessary to optimize the two-objective together with economic and thermodynamic criteria.

**Table 13** Range of decision variables and their optimal values in ACNP

| Decision variable | Range of variation | I | II |
|---|---|---|---|
| Steam inlet temperature/°C | 120–150 | 120 | 144.5 |
| Cooling water inlet temperature/°C | 25–38 | 25 | 25.03 |
| Chilled water inlet temperature/°C | 10–11 | 10.01 | 11 |
| Solution heat exchanger efficiency | 0.2–0.7 | 0.699 | 0.698 |
| Steam control valve opening/% | 50–100 | 86.43 | 70.93 |

### Two-objective optimization results

This subsection simultaneously considers two objective functions of the $ECOP_{ACN}$ (which needs to be maximized) and the $AOC_{ACNP}$ (which needs to be minimized). The first and second objective functions are similar to Eqs. (23) and (25), respectively. The operating parameters used for optimization include the network inlet cooling water temperature, the network inlet steam temperature, the network outlet chilled water temperature, the steam control valve opening percentage, network inlet steam flow rate and the solution heat exchanger efficiency. Regarding the optimization curve shown in Fig. 16a, the $ECOP_{ACN}$ and $AOC_{ACNP}$ are maximal at point I, indicating that this point is the ideal point from the exergy viewpoint. At point II, the $AOC_{ACNP}$ is minimal, implying that this point is an ideal point from an economic point of view. Figure 16b shows the Pareto frontier curve in terms of the linear normalized values of the ECOP and AOC. The LINMAP decision method selects the point with the closest distance to the ideal solution.

As shown in Figs. 16 a and b, the results of two-objective optimization method are slightly different from values obtained by one-objective optimization method because in this method both the economic and thermodynamic criteria must be met together. And from this point of view this

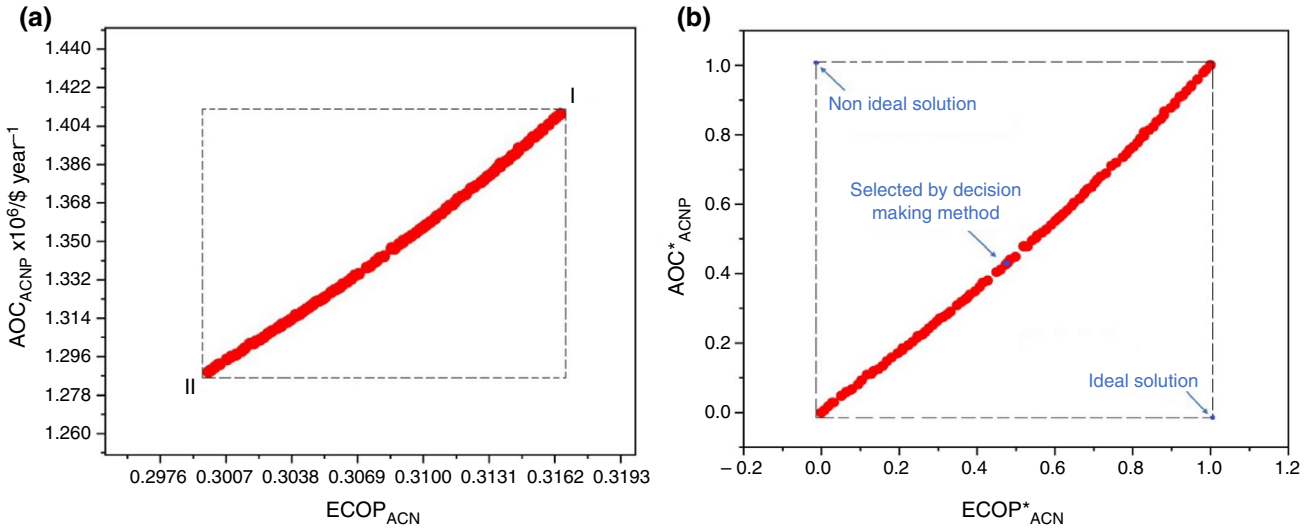


**Fig. 16** **a** MOPSO optimization results curve. **b** Pareto frontier curve normalized by the results of MOPSO optimization

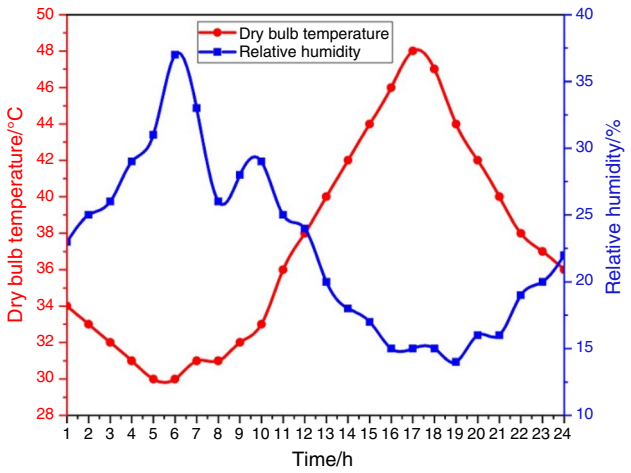


**Fig. 17** Temperature and relative humidity of Bandar-E-Mahshahr September 1, 2019

method rather than one-objective optimization method can be more efficient.

### Optimization scenarios Results

To initiate the results for the optimization technique applied to the system, it was showing the behavior of the temperature and relative humidity of environmental in a typical day in Bandar-E-Mahshahr (where the case study was located). This day was on September 1, 2019, according to Iran meteorological organization history data [81]. Figure 17 displays the temperature and relative humidity of Bandar-E-Mahshahr. To perform ACNP through coding in EES, it is assumed that the cooling load required for the two mentioned heat exchangers is constant and equal to 19,100 kW.

### Actual operation Scenario – Reference of the plant

At first, it was determining the behavior of the energetic parameters of the ACNP without the optimal operating conditions. Figure 18 shows the behavior of the inlet cooling water temperature and the electrical power consumption of ACNP's equipment with an hour for the mentioned day. It also shows the behavior of output chilled water temperature and input heat of ACN with a time for the mentioned day.

As observed in Fig. 18a, reducing the air density of the cooling tower inlet decreases the relative humidity of the ambient air, and thus, less work is required in the process. The lowest temperature of cooling water was occurred at 8 am and was 34.5 °C, and the cooling water temperature rises by increasing the air dry-bulb temperature to its maximum value of 37.75 °C at 5:30 pm.

As shown in Fig. 18b, increasing the temperature of the inlet network cooling water increases the outlet network chilled water temperature. However, when the outlet chilled water temperature is set to 10 °C, the chillers generator needs more thermal energy to maintain the outlet chilled water temperature at the set value.

Figure 19 shows the cost of consumed thermal and electrical energy of the plant in usual mode in dollars per hour for the concerned day. In this case, the cost of thermal energy consumption of the plant is more than its electrical energy cost, as shown.

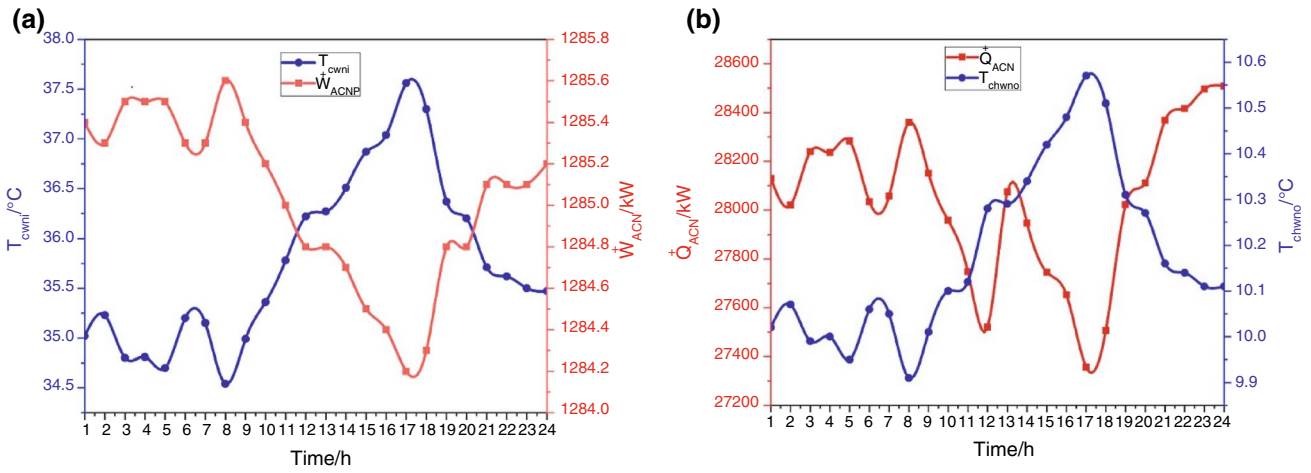


**Fig. 18** The behavior of the energetic parameter without optimal operating conditions for September 1, 2019. **a** Inlet cooling water temperature and the electrical power consumption of ACNP's equipment with an hour. **b** Output chilled water temperature and input heat of ACN with a time

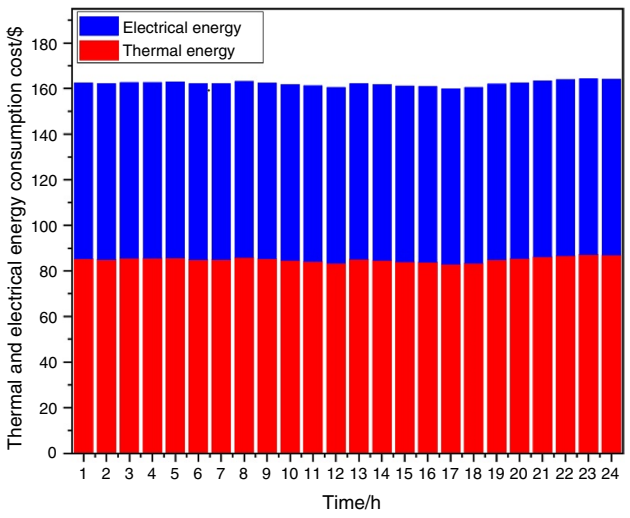


**Fig. 19** The variations of the cost of consumed thermal and electrical energy of plant in usual mode with time for September 1, 2019

## Optimal conditions – multi-objective optimization

After applying the multi-objective optimization technique according to the strategy which is shown in Fig. 6, the behavior of the energetic and financial parameters changed and it was present as follows. Figure 20 illustrates the behavior of network output chilled water temperature and heat consumption. It also illustrates the behavior of the inlet cooling water temperature and the electrical power consumption by using the optimal operating conditions considering the two-objective optimal results (See optimization results section).

As shown in Fig. 20a, by adjusting the operating conditions to the two-objective optimal state, the thermal energy required by the network is reduced compared to usual conditions. On the other hand, according to the results from Fig. 20b, reducing the temperature of the network inlet cooling water increases the electrical power consumption of the ACNP, because of switching more cooling tower fans on.

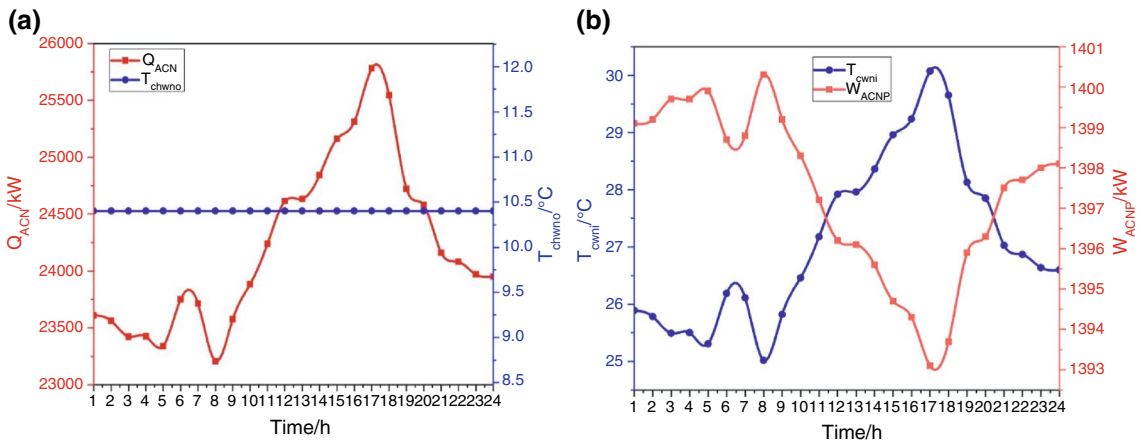


**Fig. 20** The behavior of temperature and energy parameters considering the two-objective optimal case. **a** Network output chilled water and heat consumption. **b** Inlet cooling water temperature and the electrical power consumption

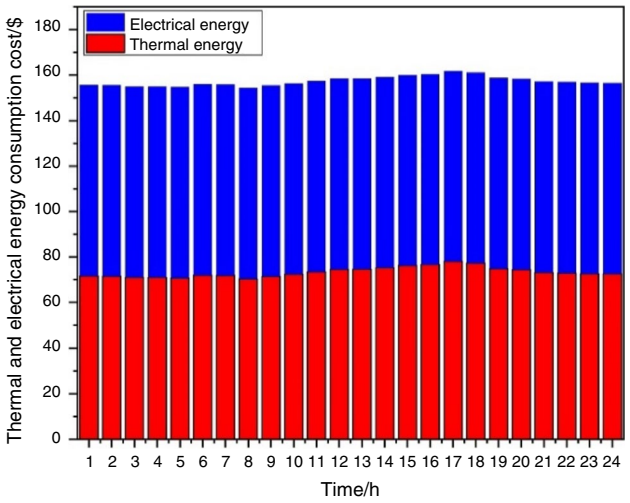


**Fig. 21** Cost of consumed thermal and electrical energy in the plant for two-objective optimal case

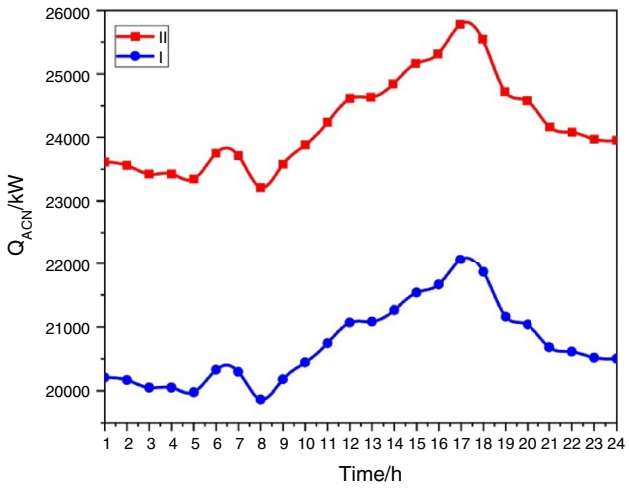


**Fig. 22** The variation of network inlet thermal energy for economically optimal case (I) and two-objective optimization case (II) over time in the mentioned day

Figure 21 illustrates the thermal and electrical power consumption in dollars per hour for the two-objective optimal condition.

In this case, the cost of electricity consumption of the plant is higher than that of fuel consumption, due to the increased number of ON cooling tower fans. However, the average cost in this case is 120 \$ $day^{-1}$ lower than that of the usual conditions, due to a significant reduction in fuel consumption.

### Optimal conditions—economical optimization case (I) and two-objective optimization case (II)

Finally, it was shown the behavior of the results of the plant when applied the optimal conditions considering two cases: economical optimization case (I) and two-objective optimization case (II). Figure 22 illustrates the plant thermal energy consumption for the two cases.

As shown, the thermal energy consumption of the plant in the economical optimization case is less than that of the two-objective optimization case, because all decision variables are economically optimal.

To demonstrate the thermal and electrical power consumption for the economical optimization case, Fig. 23 shows the behavior of those energy parameters in dollars on the desired day. As it shows, the average cost of the plant is reduced to 368 \$ $day^{-1}$ in the economically optimal case.

A case study was conducted on an industrial ACNP with high thermal and electrical energy consumption. Changing the flow rate of cooling and chilled water pumps with variable frequency derived for these pumps with high electrical power requirement is not feasible and affordable now, because of technical shortage. Therefore, in this study, for this kind of plants we proposed a simple and applicable method which relies on obtaining optimal operating condition with an innovative method described in the flowchart shown in Fig. 6. Applying this method as can be seen in the results in addition to increasing the exergy performance coefficient significantly reduces the annual cost of the plant. Also, this method can help the operators to predict the optimum operating conditions of the ACNP for each month of the year.

## Comparison of the results against the literature

This section compares the results of the present study with the literature. It is worthy to mention energy, exergy and economic analysis of the single-effect ACNP which is

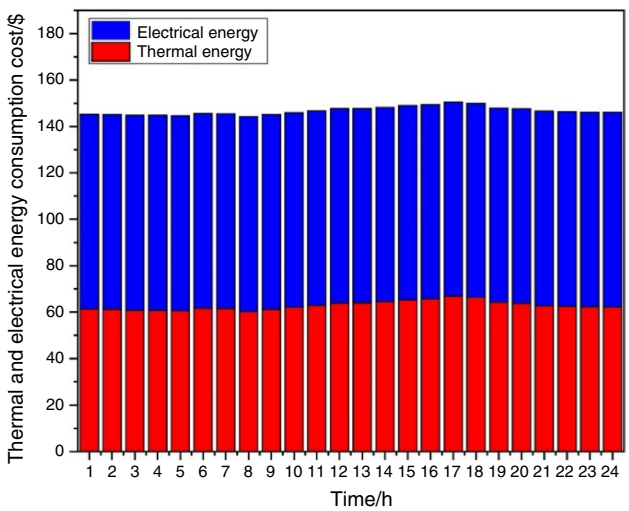


**Fig. 23** Cost of consuming thermal and electrical power of plant for economically optimal case over time in the mentioned day

**Table 14** Comparison of the results of the present study in the literature

| Author | Year | Case study | Parameters studied and key finding | Present study |
|---|---|---|---|---|
| *Energy analysis* | | | | |
| Thangavelu et al. [50] | 2017 | Chiller plant with two absorption chillers (2307 kW) and one centrifugal chiller (4200 kW) | The effect of using variable speed pumps for chilled and cooling water and optimizing the temperature of the chilled and cooling water set points in the plant's electrical energy consumption<br>It causes a 40% reduction in the plant's electrical energy consumption | By considering the efficiency of a gas power plant equals to 40% for generating electricity and converting the amount of thermal energy consumption of considered ACNP to electrical energy, the proposed method in the optimal economic mode without the use of variable speed pumps causes a 23% reduction in the electrical energy consumption of the plant |
| Sheikhani et al. [21] | 2018 | Solar absorption cooling systems integrated with auxiliary energy sources (review paper) | COP, annual energy consumption cost and the payback period of solar absorption chiller investment by choosing different solar collectors. For the single-effect steam absorption chiller when an inlet steam temperature increases more than 100 °C, COP is almost constant | The COP along the whole range of steam temperature is approximately constant because the COP varies from 66.96% to 66.79% which was practically the same |
| Wang et al. [83] | 2017 | Steady-state and dynamic modeling of single-effect LiBr/$H_2o$ absorption chiller with 10 kW cooling capacity | The effect of the cooling water, chilled water and hot water on the relaxation time and COP<br>As the hot water temperature rises from 90 to 105 °C, the COP first rises and then be constant<br>Increasing the temperature of the inlet cooling water causes a significant decrease in the COP<br>Increasing the inlet chilled water temperature of the evaporator increases the COP | Increasing the inlet chilled water temperature and reducing the inlet cooling water temperature increase COP |
| *Exergy analysis* | | | | |
| Mastani Joybari and Haghighat [84] | 2016 | Steady-state modeling of single-effect LiBr/$H_2o$ absorption chiller with 14 kW cooling capacity | The effect of flow and temperature of inlet hot, cooling and chilled water on the destruction of exergy in various chiller absorption heat exchangers<br>Reducing the inlet flowrate reduces the destruction of the exergy in various chiller heat exchangers. Reducing the inlet steam temperature and the outlet chilled water temperature of the chiller increases the exergetic efficiency of the chiller | Reducing the inlet steam temperature and the outlet chilled water temperature increases the exergetic efficiency of the chiller |

**Table 14** (continued)

| Author | Year | Case study | Parameters studied and key finding | Present study |
|---|---|---|---|---|
| Lake et al. [85] | 2017 | Absorption chiller network plant included one single-effect absorption chiller (2208 kW), steam boiler (10.43 MW), cooling tower (2391 kW) and thermal storage tank (7500 $m^3$) | Investigating the exergetic efficiency of the absorption chiller plant<br>Plant exergetic efficiency was about 16%.<br>Absorber and generator have the highest exergy destruction | The exergetic efficiency of the ACN in this study is approximately 21% in the design condition. Absorber and evaporator have the highest exergy destruction. The exergy destruction of the generator was obtained less than other components in this study, as the drain heat exchanger installed at the generator output was considered as part of the generator. Therefore, the thermal energy of the steam was completely absorbed by LiBr/$H_2O$ solution and then exited from the chiller as condensed steam. The quality and temperature of outlet steam are the two factors that significantly affect the exergy destruction in the absorber and generator of the chiller |
| *Economy analysis* | | | | |
| Abbaspour and Saraei [86] | 2014 | Steady-state modeling of single-effect LiBr/$H_2o$ absorption chiller with 14 kW cooling capacity | Optimization of single-effect chiller performance using a genetic algorithm. Thermodynamic optimization reduces the total cost rate by 12% | Thermodynamic optimization of the ACNP reduces the annual cost of 3.24% |

compromised electrical and thermal energy consumption same as the present study, according to the open literature has not previously been performed. In Table 14, the results of previous studies related to this paper topic are reported.

## Conclusions

The desirable network was analyzed parametrically from the viewpoint of energy, exergy and economic analysis. Then, the network was optimized to maximize exergy performance coefficient and minimize annual cost. The multi-objective optimization was implemented using the MOPSO algorithm. Ultimately, the effect of operational parameters including network inlet cooling water temperature, steam temperature, steam flow rate, network outlet chilled water temperature and the efficiency of solution heat exchanger on the $COP_{ACN}$, $ECOP_{ACN}$ and $AOC_{ACNP}$ was evaluated. The following outlines could be summarized as a conclusion:

(a) Findings of the energy analysis;

- Increasing the efficiency of the ACN's solution heat exchangers or a reduction in the ACN inlet cooling water temperature increases $COP_{ACN}$.
- An increase in the ACN inlet steam temperature reduces $COP_{ACN}$ and decreases the ACN outlet chilled water temperature.

(b) Findings of exergy analysis

- Increasing efficiency of the ACN's solution heat exchangers increases $ECOP_{ACN}$ and exergy destruction of the ACN's evaporators.
- Reducing the ACN inlet cooling water temperature generally increases $ECOP_{ACN}$ and decreases the exergy destruction of the ACN's chillers.
- ACN and cooling tower have the highest exergy destruction in the ACN plant.

(c) Findings of economy analysis

- Generally, decreasing the ACN inlet cooling water temperature reduces the $AOC_{ACNP}$, due to declined steam consumption of the plant.
- Increasing the ACN outlet chilled water temperature reduces the $AOC_{ACNP}$, due to reduced steam consumption of the plant.
- An increase in the efficiency of the ACN's solution heat exchangers reduces the $AOC_{ACNP}$, due to reduced steam consumption of the plant.

(d) Findings of optimization analysis

- When the ACN works in optimal economic conditions, $AOC_{ACNP}$ reduces to 9.95%
- When the ACN operates in optimal thermodynamic and economic conditions, $AOC_{ACNP}$ decreases to 3.24%

**Acknowledgement** The authors express their thanks to the department of research and innovation of the M.P.C. for the technical support in this research. The fourth author thanks the CNPq for the scholarship of Productivity nº 309154/2019-7 and the IFPE for its financial support throughout the Call 10/2019/Propesq. The fourth author also thanks FACEPE/CNPq for financial support for research project APQ-0151-3.05/14 and the CNPq for financial support for the research project - Universal 402323/2016-5.

## Appendix

The empirical equation is used to model the cooling tower as follows [61]:

$$\begin{aligned}\text{Approach} = {} & C_1 + C_2 \times FR_a + C_3 \times FR_a^2 + C_4 \times FR_a^3 + C_5 \times FR_w + C_6 \times FR_a \times FR_w + C_7 \times FR_a^2 \times FR_w \\ & + C_8 \times FR_w^2 + C_9 \times FR_a \times FR_w^2 + C_{10} \times FR_w^3 + C_{11} \times T_{wb} + C_{12} \times FR_a \times T_{wb} + C_{13} \times FR_a^2 \times T_{wb} + C_{14} \times T_{wb} \\ & \times FR_w + C_{15} \times FR_a \times FR_w \times T_{wb} + C_{16} \times T_{wb} \times FR_w^2 + C_{17} \times T_{wb}^2 + C_{18} \times T_{wb}^2 \times FR_a + C_{19} \\ & \times T_{wb}^2 \times FR_w + C_{20} \times T_{wb}^3 + C_{21} \times Tr + C_{22} \times FR_a \times Tr + C_{23} \times FR_a^2 \times Tr + C_{24} \times FR_w \\ & \times Tr + C_{25} \times FR_a \times FR_w \times Tr + C_{26} \times FR_w^2 \times Tr + C_{27} \times T_{wb} \times Tr + C_{28} \times T_{wb} \times FR_a \times Tr \\ & + C_{29} \times FR_w \times Tr \times T_{wb} + C_{30} \times T_{wb}^2 \times Tr + C_{31} \times Tr^2 + C_{32} \times Tr^2 \times FR_a + C_{33} \times Tr^2 \\ & \times FR_w + C_{34} \times T_{wb} \times Tr^2 + C_{35} \times Tr^3\end{aligned}$$

Approach = approach temperature (°C) = outlet cooling tower water temperature minus inlet cooling tower air wet-bulb temperature

$FR_a$ = air flow rate ratio (cooling tower actual air flow rate divided by design air flow rate)

$FR_w$ = water flow rate ratio (cooling tower actual water flow rate divided by design water flow rate)

Tr = range temperature (°C) = inlet cooling tower water temperature minus outlet water temperature

$T_{wb}$ = inlet cooling tower air wet-bulb temperature (°C)

Table of approach temperature correlation coefficients [61]

| | | | | | |
|---|---|---|---|---|---|
| $C_1$ | 0.52049709836241 | $C_{17}$ | − 0.00270968955115 | $C_{33}$ | − 0.01858546718156 |
| $C_2$ | − 10.617046395344 | $C_{18}$ | 0.00112277498589 | $C_{34}$ | 0.00115667701294 |
| $C_3$ | 10.7292974722538 | $C_{19}$ | − 0.00127758497498 | $C_{35}$ | 0.00080737066446 |
| $C_4$ | − 2.74988377158227 | $C_{20}$ | 7.60420796601607E − 05 | | |
| $C_5$ | 4.73629943913743 | $C_{21}$ | 1.43600088336017 | | |
| $C_6$ | − 8.25759700874711 | $C_{22}$ | − 0.5198695909109 | | |
| $C_7$ | 1.57640938114136 | $C_{23}$ | 0.11733957691051 | | |
| $C_8$ | 6.51119643791324 | $C_{24}$ | 1.50492810819924 | | |
| $C_9$ | 1.50433525206692 | $C_{25}$ | − 0.13589890592697 | | |
| $C_{10}$ | − 3.2888529287801 | $C_{26}$ | − 0.15257758186651 | | |
| $C_{11}$ | 0.02577861453538 | $C_{27}$ | − 0.05338438281146 | | |
| $C_{12}$ | 0.18246428931525 | $C_{28}$ | 0.00493294869566 | | |
| $C_{13}$ | − 0.08189472914009 | $C_{29}$ | − 0.00796260394174 | | |
| $C_{14}$ | − 0.21501000399629 | $C_{30}$ | 0.00022261982862 | | |
| $C_{15}$ | 0.01867413096353 | $C_{31}$ | − 0.05439520015681 | | |
| $C_{16}$ | 0.053682417759 | $C_{32}$ | 0.00474266879162 | | |

## References


1. Cui P, Yu M, Liu Z, Zhu Z, Yang S. Energy, exergy, and economic (3E) analyses and multi-objective optimization of a cascade absorption refrigeration system for low-grade waste heat recovery. Energy Convers Manag. 2019;184:249–61. https://doi.org/10.1016/j.enconman.2019.01.047.
2. Ochoa AAV, Dutra JCC, Henriquez JRG, Dos Santos CAC, Rohatgi J. The influence of the overall heat transfer coefficients in the dynamic behavior of a single effect absorption chiller using the pair LiBr/$H_2O$. Energy Convers Manag. 2017;136:270–82. https://doi.org/10.1016/j.enconman.2017.01.020.
3. Esen H, Inalli M, Esen M. Technoeconomic appraisal of a ground source heat pump system for a heating season in eastern Turkey. Energy Convers Manag. 2006;47:1281–97. https://doi.org/10.1016/j.enconman.2005.06.024.
4. Esen H, Inalli M, Esen M, Pihtili K. Energy and exergy analysis of a ground-coupled heat pump system with two horizontal ground heat exchangers. Build Environ. 2007;42:369–80. https://doi.org/10.1016/j.buildenv.2006.10.014.
5. Ochoa AAV, Dutra JCC, Guerrero JRH, Dos Santos CAC, Costa JAPD. Dynamic experimental analysis of a LiBr/$H_2O$ single effect absorption chiller with nominal capacity of 35 kW of cooling. Acta Scient Technol. 2019;41:1–11. https://doi.org/10.4025/actascitechnol.v41i1.35173.
6. Ahmadi P, Hamut HS, Ghaffarizadeh A, Hanafizadeh P, Ghasemi-sahebi E. Exergetic optimization of power generation systems. Int J Chem Eng. 2016. https://doi.org/10.1155/2016/3962847.
7. James A, Mohanraj M, Srinivas M, Jayaraj S. Thermal analysis of heat pump systems using photovoltaic-thermal collectors: a review. Journal of Thermal Analysis and Calorimetry. 2020:1-39. https://doi.org/10.1007/s10973-020-09431-2.
8. Ochoa AAV, Dutra JCC, Henriquez JRG, Dos Santos CAC. Techno-economic and exergoeconomic analysis of a micro cogeneration system for a residential use. Acta Scient Technol. 2016;38:327–38. https://doi.org/10.4025/actascitechnol.v38i3.28752.
9. Ehyaei MA, Ahmadi A, Haj Assad MA, Rosen M. Investigation of an integrated system combining an organic Rankine cycle and absorption chiller driven by geothermal energy: energy, exergy, and economic analyses and optimization. J Clean Prod. 2020;258:120780. https://doi.org/10.1016/j.jclepro.2020.120780.
10. Ochoa AAV, Dutra JCC, Henriquez JRG, Dos Santos CAC, Rohatgi J. Energetic and exergetic study of a 10 RT absorption chiller integrated into a microgeneration system. Energy Convers Manag. 2014;18:545–53. https://doi.org/10.1016/j.enconman.2014.08.064.
11. Maryami R, Dehghan AA. An exergy based comparative study between LiBr/water absorption refrigeration systems from half effect to triple effect. Appl Therm Eng. 2017;124:103–23. https://doi.org/10.1016/j.applthermaleng.2017.05.174.
12. Petela K, Szlek A. Energy and exergy analysis of solar heat driven chiller under wide system boundary conditions. Energy. 2019;168:440–9. https://doi.org/10.1016/j.energy.2018.11.067.
13. Ehyaei MA, Ahmadi AA, Rosen M. Energy, exergy, economic and advanced and extended exergy analyses of a wind turbine. Energy Convers Manag. 2019;183:369–81. https://doi.org/10.1016/j.enconman.2019.01.008.
14. Yuan B, Zhang Y, Wenli D, Meihong W, Qian F. Assessment of energy saving potential of an industrial ethylene cracking furnace using advanced exergy analysis. Appl Energy. 2019;254:113583. https://doi.org/10.1016/j.apenergy.2019.113583.
15. Esen H, Inalli M, Esen M. A techno-economic comparison of ground-coupled and air-coupled heat pump system for space cooling. Build Environ. 2007;42:1955–65. https://doi.org/10.1016/j.buildenv.2006.04.007.
16. Esen M, Yuksel T. Experimental evaluation of using various renewable energy sources for heating a greenhouse. Energy Build. 2013;65:340–51. https://doi.org/10.1016/j.enbuild.2013.06.018.
17. Silva HCN, Dutra JCC, Costa JAP, Ochoa AAV, Dos Santos CAC, Araujo MMD. Modeling and simulation of cogeneration systems for buildings on a university campus in north east Brazil – a case study. Energy Convers Manag. 2019;186:334–48. https://doi.org/10.1016/j.enconman.2019.02.062.
18. Lubis A, Jeong J, Giannetti N, Yamaguchi S, Saito K, Yabase H, Alhamid MI, Nasruddin. Operation performance enhancement of single-double-effect absorption chiller. Appl Energy. 2018;219:299–311. https://doi.org/10.1016/j.apenergy.2018.03.046.
19. Lu D, Bai Y, Zhao Y, Dong X, Gong M, Luo E, Chen G, Xu Q, Shen J. Experimental investigations of an absorption heat pump prototype with intermediate process for residential district heating. Energy Convers Manag. 2020;204:12323. https://doi.org/10.1016/j.enconman.2019.112323.
20. Alcantara SCS, Ochoa AAV, da Costa JAP, Michima PSA, Silva HCN. Natural gas based trigeneration system proposal to an ice cream factory: an energetic and economic assessment. Energy Convers Manag. 2019;197:111860. https://doi.org/10.1016/j.enconman.2019.111860.
21. Sheikhani H, Barzegarian R, Heydari A, Kianifar A, Kasaeian A, Grof G, Mahian O. A review of solar absorption cooling systems combined with various auxiliary energy devices. J Therm Anal Calorim. 2018;134:2197–212. https://doi.org/10.1007/s10973-018-7423-4.
22. Xu H, Zhang Z, Hu Z, Dai X, Wang J, Jiao W, et al. Thermodynamic and economic analysis of a micro-combined polygeneration system coupled with solar energy and fuels for distributed applications. J Therm Anal Calorim. 2020. https://doi.org/10.1007/s10973-020-09799-1.
23. Shirazi AA, Taylor RL, Morrison GD, White S. Solar-powered absorption chillers: a comprehensive and critical review. Energy Convers Manag. 2018;171:59–81. https://doi.org/10.1016/j.enconman.2018.05.091.
24. Sokhansefat T, Mohammadi D, Kasaeian A, Mahmoudi AR. Simulation and parametric study of a 5-ton solar absorption cooling system in Tehran. Energy Convers Manag. 2017;148:339–51. https://doi.org/10.1016/j.enconman.2017.05.070.
25. Arabkoohsar A, Andresen GB. A smart combination of a solar assisted absorption chiller and a power productive gas expansion unit for cogeneration of power and cooling. Renewable Energy. 2018;115:489–500. https://doi.org/10.1016/j.renene.2017.08.069.
26. Arabkoohsar A, Sadi M. Technical comparison of different solar-powered absorption chiller designs for co-supply of heat and cold networks. Energy Convers Manag. 2020;206:112343. https://doi.org/10.1016/j.enconman.2019.112343.
27. Esen H, Esen M, Ozsolak O. Modelling and experimental performance analysis of solar-assisted ground source heat pump system. J Exp Theor Artif Intell. 2017;29(1):1–17. https://doi.org/10.1080/0952813X.2015.1056242.
28. Jani DB, Bhabhor K, Dadi M, Doshi S, Jotaniya PV, Ravat H, et al. A review on use of TRNSYS as simulation tool in performance prediction of desiccant cooling cycle. J Therm Anal Calorim. 2020;140:2011–31. https://doi.org/10.1007/s10973-019-08968-1.
29. Cai W, Li X, Maleki A, Pourfayaz F, Rosen MA, Nazari MA, et al. Optimal sizing and location based on economic parameters for an off-grid application of a hybrid system with photovoltaic, battery and diesel technology. Energy. 2020;201:117480. https://doi.org/10.1016/j.energy.2020.117480.
30. Maleki A, Nazari MA, Pourfayaz F. Harmony search optimization for optimum sizing of hybrid solar schemes based on battery

storage unit. Energy Reports. 2020. https://doi.org/10.1016/j.egyr.2020.03.014.
31. Jagtap H, Bewoor A, Kumar R, Ahmadi MH, Lorenzini G. Markov-based performance evaluation and availability optimization of the boiler–furnace system in coal-fired thermal power plant using PSO. Energy Reports. 2020;6:1124–34. https://doi.org/10.1016/j.egyr.2020.04.028.
32. Sadaghiani MS, Ahmadi MH, Mehrpooya M, Pourfayaz F, Feidt M. Process development and thermodynamic analysis of a novel power generation plant driven by geothermal energy with liquefied natural gas as its heat sink. Appl Therm Eng. 2018;133:645–58. https://doi.org/10.1016/j.applthermaleng.2018.01.077.
33. Pakatchian MR, Saeidi H, Ziamolki A. CFD-based blade shape optimization of MGT-70(3) axial flow compressor. International Journal of Numerical Methods for Heat and Fluid Flow. 2019; ahead-of-print:7. https://doi.org/10.1108/hff-10-2018-0603.
34. Pandya B, Kumar V, Matawala V, Pate J. Thermal comparison and multi-objective optimization of single-stage aqua-ammonia absorption cooling system powered by different solar collectors. J Therm Anal Calorim. 2018;133:1635–48. https://doi.org/10.1007/s10973-018-7193-z.
35. Pandya B, Modi N, Kumar V, Upadhyai R, Patel J. Performance comparison and optimal parameters evaluation of solar assisted NH3–NaSCN and NH3–LiNO3 type absorption cooling system. J Therm Anal Calorim. 2018;134:3437–52. https://doi.org/10.1007/s10973-018-7561-8.
36. Karami M, Wang L. Particle swarm optimization for control operation of an all-variable speed water-cooled chiller plant. Appl Therm Eng. 2018;130:962–78. https://doi.org/10.1016/j.applthermaleng.2017.11.037.
37. Cezar KL, Caldas AGA, Caldas AMA, Cordeiro MCL, Dos Santos CAC, Ochoa AAV, Michima PSA. Development of a novel flow control system with arduino microcontroller embedded in double effect absorption chillers using the LiBr/$H_2O$ pair. Int J Refrig. 2020;111:124–35. https://doi.org/10.1016/j.ijrefrig.2019.11.014.
38. Mu B, Li YM, House JI, Salsbury T. Real-time optimization of a chilled water plant with parallel chillers based on extremum seeking control. Appl Energy. 2017;208:766–81. https://doi.org/10.1016/j.apenergy.2017.09.072.
39. Huang S, Zuo W, Sohn MD. Amelioration of the cooling load-based chiller sequencing control. Appl Energy. 2016;168:204–15. https://doi.org/10.1016/j.apenergy.2016.01.035.
40. Wang L, Lee EWM, Yuen RKK, Feng W. Cooling load forecasting-based predictive optimization for chiller plants. Energy Build. 2019;198:261–74. https://doi.org/10.1016/j.enbuild.2019.06.016.
41. Sabbaghm A, Gomez JM. Optimal control of single stage LiBr/water absorption chiller. Int J Refrig. 2018;92:1–9. https://doi.org/10.1016/j.ijrefrig.2018.05.007.
42. Ghorbani B, Kowsary F, Ebrahimi S, Vijayaraghavan K. CFD modeling and optimization of a latent heat storage unit for running a solar assisted single effect Li-Br absorption chiller using multi-objective genetic algorithm. Sustain Cities Soc. 2017;34:321–34. https://doi.org/10.1016/j.scs.2017.05.023.
43. Zheng Z, Li J, Duan P. Optimal chiller loading by improved artificial fish swarm algorithm for energy saving. Math Comput Simul. 2018;12:12. https://doi.org/10.1016/j.matcom.2018.04.013.
44. Huang S, Zuo WD, Sohn M. A Bayesian network model for predicting cooling load of commercial buildings. Build Simul. 2018;11:87–101. https://doi.org/10.1007/s12273-017-0382-z.
45. Nasruddin, Sholahudin S, Alhamid MI, Saito K. Hot water temperature prediction using a dynamic neural network for absorption chiller application in Indonesia. Sustain Energy Technol Assessm. 2018;30:114–20. https://doi.org/10.1016/j.seta.2018.09.006.
46. Ochoa AAV, Dutra JCC, Henriquez JRG, Dos Santos CAC. Dynamic study of a single effect absorption chiller using the pair LiBr/$H_2O$. Energy Convers Manag. 2016;108:30–42. https://doi.org/10.1016/j.enconman.2015.11.009.
47. Dincer I, Rosen MA, Ahmadi P. Optimization of energy systems. John Wiley & Sons Ltd. 2017.
48. Ahmadi P, Dincer I. Energy optimization. Comprehen Energy Syst. 2018;1:1085–143. https://doi.org/10.1016/B978-0-12-809597-3.00135-8.
49. Thermax products, Absorption systems, Absorption chillers. 2016. http://www.thermaxglobal.com.
50. Thangavelu SR, Myat A, Khambadkone A. Energy optimization methodology of multi-chiller plant in commercial buildings. Energy. 2017;123:64–76. https://doi.org/10.1016/j.energy.2017.01.116.
51. Ahmadi MH, Mehrpooya M, Pourfayaz F. Exergoeconomic analysis and multi objective optimization of performance of a carbon dioxide power cycle driven by geothermal energy with liquefied natural gas as its heat sink. Energy Convers Manag. 2016;119:422–34. https://doi.org/10.1016/j.enconman.2016.04.062.
52. Ebrahimi-Moghadam A, Jabari Moghadam A, Farzaneh-Gord M, Aliakbari K. Proposal and assessment of a novel combined heat and power system: energy, exergy, environmental and economic analysis. Energy Convers Manag. 2020;204:112307. https://doi.org/10.1016/j.enconman.2019.112307.
53. Sanaye S, Amani M, Amani P. 4E modeling and multi criteria optimization of CCHPW gas turbine plant with inlet air cooling and steam injection. Sustain Energy Technol Assessm. 2018;29:70–81. https://doi.org/10.1016/j.seta.2018.06.003.
54. Jain V, Sachdeva G. Energy, exergy, economic (3E) analyses and multi-objective optimization of vapor absorption heat transformer using NSGA-II technique. Energy Convers Manag. 2017;148:1096–113. https://doi.org/10.1016/j.enconman.2017.06.055.
55. F-chart software, Engineering equations solver (EES). 2016. Version 10.09.
56. Huang S, Zuo WD, Sohn M. Improved cooling tower control of legacy chiller plants by optimizing the condenser water set point. Build Environ. 2017;111:33–46. https://doi.org/10.1016/j.buildenv.2016.10.011.
57. Stull R. Wet-bulb temperature from relative humidity and air temperature. Am Meteorol Soc. 2011. https://doi.org/10.1175/JAMC-D-11-0143.1.
58. Gao M, Sun FZ, Zhou SJ, Shi YT, Zhao YB, Wang NH. Performance prediction of wet cooling tower using artificial neural network under crosswind conditions. Int J Therm Sci. 2009;48:583–9. https://doi.org/10.1016/j.ijthermalsci.2008.03.012.
59. Jin GY, Cai WJ, Lu L, Lee E, Chiang A. A simplified modeling of mechanical cooling tower for control and optimization of HVAC systems. Energy Convers Manag. 2007;48:355–65. https://doi.org/10.1016/j.enconman.2006.07.010.
60. Wang JG, Shieh SS, Jang SS, Wong DH, Wu CW. Data-driven modeling approach for performance analysis and optimal operation of a cooling tower. J Taiw Inst of Chem Eng. 2014;45:180–5. https://doi.org/10.1016/j.jtice.2013.05.012.
61. Simulation models – Encyclopedic reference. Energy plus documentation. 2019.
62. Wang L, Lee EWM, Yuen RKK. A practical approach to chiller plants optimization. Energy Build. 2018;169:332–43. https://doi.org/10.1016/j.enbuild.2018.03.076.
63. Liu Z, Tan H, Luo D, Yu G, Li J, Li Z. Optimal chiller sequencing control in an office building considering the variation of chiller maximum cooling capacity. Energy Build. 2017;140:430–42. https://doi.org/10.1016/j.enbuild.2017.01.082.
64. Dalibard A, Biesinger A, Cotrado M, Trinkle A, Bartels U, Eicker U. Performance improvement of a large chilled-water plant by

using simple heat rejection control strategies. Int J Refrig. 2018;94:1–10. https://doi.org/10.1016/j.ijrefrig.2018.07.020.
65. Myat A, Thu K, Kim YD, Chakraborty A, Chun WG, Kim Choon K. A second law analysis and entropy generation minimization of an absorption chiller. Appl Therm Eng. 2011;31:2405–13. https://doi.org/10.1016/j.applthermaleng.2011.04.004.
66. Kim Choon K, Chakraborty A, Aye SM, Xiaolin W. New pool boiling data for water with copper foam metal at sub-atmospheric pressure: experiments and correlation. Appl Therm Eng. 2006;26:1286–90. https://doi.org/10.1016/j.applthermaleng.2005.10.028.
67. Florides GA, Kalogirou SA, Tassou SA, Wrobel LC. Design and construction of a LiBr–water absorption machine. Energy Convers Manag. 2003;44:2483–508. https://doi.org/10.1016/S0196-8904(03)00006-2.
68. MATLAB™ Software. The Math works Inc., Version 2016.
69. Toghyani S, Kasaeian A, Ahmadi MH. Multi-objective optimization of Stirling engine using non-ideal adiabatic method. Energy Convers Manag. 2014;80:54–62. https://doi.org/10.1016/j.enconman.2014.01.022.
70. Ahmadi MH, Sayyaadi H, Dehghani S, Hosseinzade H. Designing a solar powered Stirling heat engine based on multiple criteria: maximized thermal efficiency and power. Energy Convers Manag. 2013;75:282–91. https://doi.org/10.1016/j.enconman.2013.06.025.
71. Nazemzadegan MR, Kasaeian A, Toghyani S, Ahmadi MH, Saidur R, Ming T. Multi-objective optimization in a finite time thermodynamic method for dish-Stirling by branch and bound method and MOPSO algorithm. Front Energy. 2018;10:1–17. https://doi.org/10.1007/s11708-018-0548-0.
72. Arora R, Kaushik SC, Kumar R, Arora R. Multi-objective thermo-economic optimization of solar parabolic dish Stirling heat engine with regenerative losses using NSGA-II and decision making. Int J Electr Power Energy Syst. 2016;74:25–35. https://doi.org/10.1016/j.ijepes.2015.07.010.
73. Liu G. Development of a general sustainability indicator for renewable energy systems: a review. Renew Sustain Energy Rev. 2014;31:611–21. https://doi.org/10.1016/j.rser.2013.12.038.
74. Bellman RE, Zadeh LA. Decision-making in a fuzzy environment: NASA contractor report. 1970. Contract no.: NASA cr-1594.
75. Yu P-L. Multiple-criteria decision making: concepts, techniques, and extensions. Springer. 1985; 383. https://doi.org/10.1007/978-1-4684-8395-6.
76. Olson DL. Decision aids for selection problems. New York: Springer; 1996.
77. Sanaye S, Farvizi A, Refahi AH, Rafieinejad MV. A novel application of optimization and computational fluid dynamics methods for designing combined ejector-compressor refrigeration cycle. Int J Refrig. 2019;108:174–89. https://doi.org/10.1016/j.ijrefrig.2019.06.006.
78. Ferrara M, Rasouli S, Khademi M, Salimi M. A robust optimization model for a decision-making problem: an application for stock market. Oper Res Perspect. 2017;4:136–41. https://doi.org/10.1016/j.orp.2017.10.001.
79. E. Herold K, Radermacher R, A. Klein S. Absorption chillers and heat pumps. 2016; CRC Press. ISBN 9781498714341.
80. Natural gas price (Henry Hub). 2019. https://origin.markets.businessinsider.com/commodities/natural-gas-price.
81. IRIMO, The weather information for Bandar-E- Mahshahr, 2019, http://www.irimo.ir.
82. How to calculate the true cost of steam, U.S. Department of Energy, Energy Efficiency and Renewable Energy 2003.
83. Wang J, Shang S, Li X, Wang B, Wu W, Shi W. Dynamic performance analysis for an absorption chiller under different working conditions. Appl Sci. 2017;7:797–815. https://doi.org/10.3390/app7080797.
84. Mastani Joybari M, Haghighat F. Exergy analysis of single effect absorption refrigeration systems: the heat exchange aspect. Energy Convers Manag. 2016;126:799–810. https://doi.org/10.1016/j.enconman.2016.08.029.
85. Lake A, Rezaie B, Beyerlein S. Use of exergy analysis to quantify the effect of lithium bromide concentration in an absorption chiller. Entropy. 2017;19:156–73. https://doi.org/10.3390/e19040156.
86. Abbaspour M, Saraei AR. Thermoeconomic analysis and multi-objective optimization of a LiBr-water absorption refrigeration system. Int J Environ Res. 2015;9:61–8. https://doi.org/10.22059/IJER.2015.874.